区域尺度温室气体模拟与反演

Xiao-Ming Hu (xhu@ou.edu)
https://caps.ou.edu/xhu/

Center for Analysis and Prediction of Storms
University of Oklahoma

2023年11月 @ 长沙

1. **3D WRF-CO_2 simulation**

Over US and China

2. **Multi-Model investigation of Haze Pollution**
3. **WRF-GHG for both CO_2 and CH_4 simulation**
4. **CH4 inversion**

Trend of CO_2

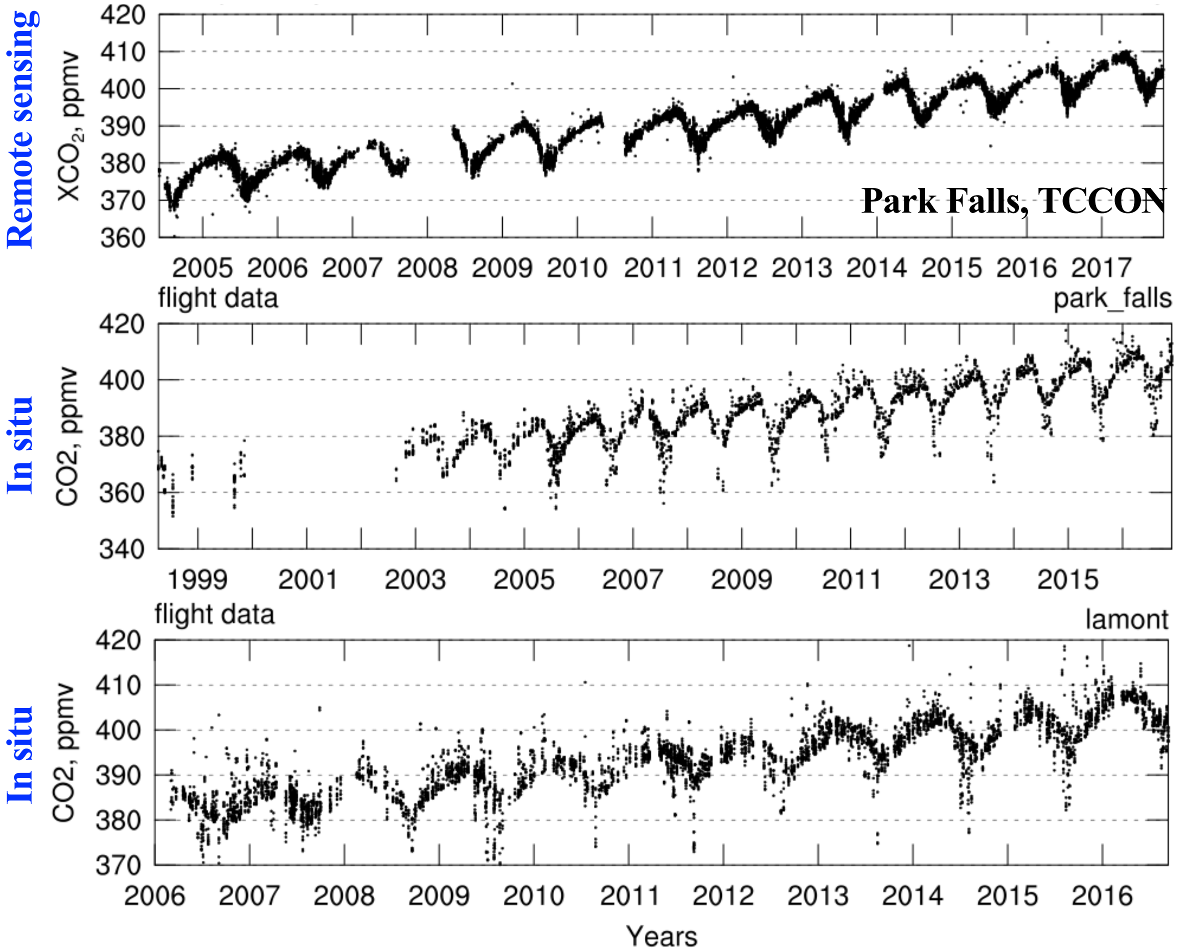

Global warming controversial? Look at CO_2 trend!!

Global CO_2 sources and sinks

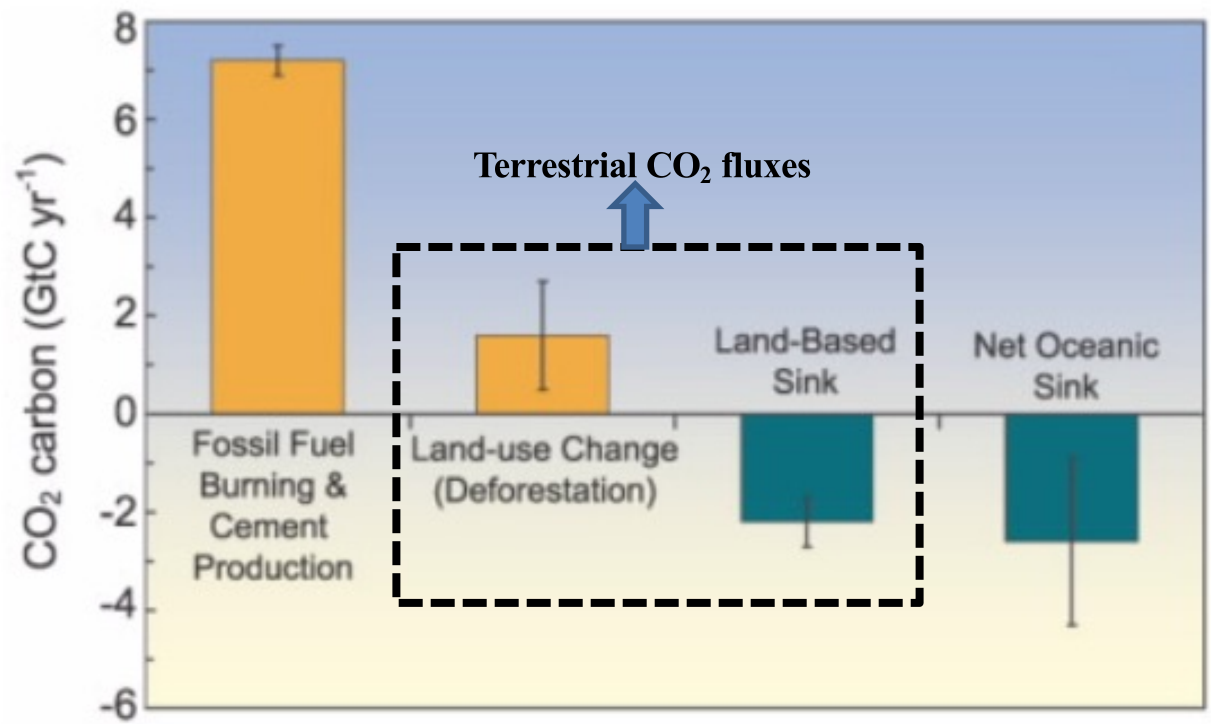

IPCC (2007)

Uncertainties of terrestrial CO_2 fluxes are large

Terrestrial CO_2 fluxes in different regions

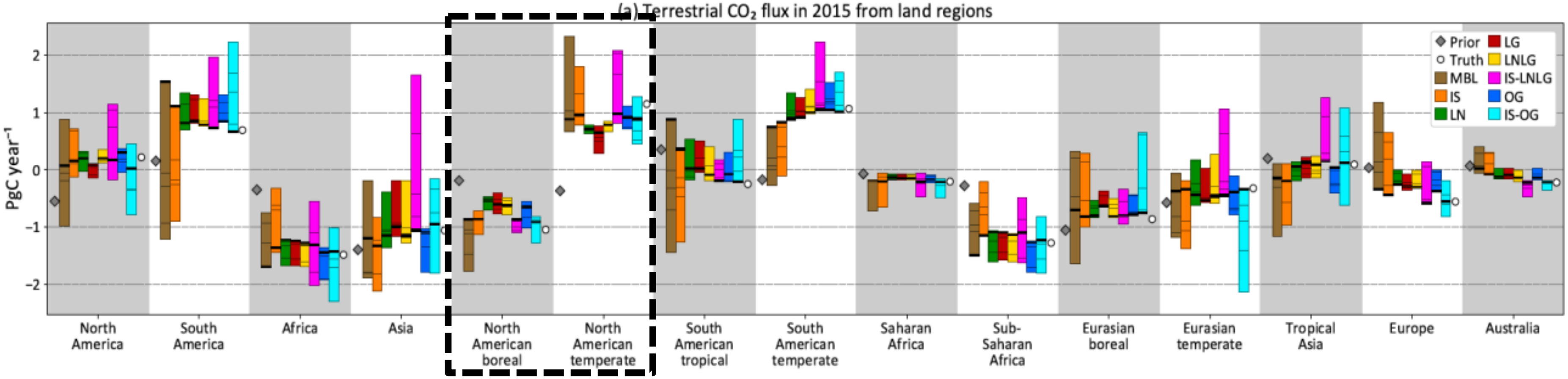

(Sourish Basu et al., 2018)

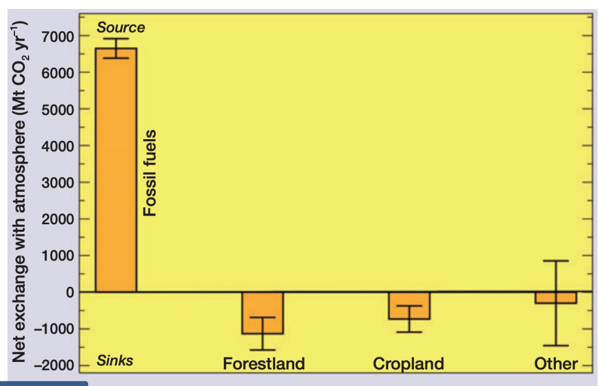

North American CO_2 sources and sinks, circa 2010. The fossi

King et al., 2012

Uncertainties in each region/plant function are large too

Weather-biosphere online-coupled WRF-VPRM

- Vegetation Photosynthesis and Respiration Model (VPRM) (Xiao et al., 2004; Mahadevan et al., 2008; Ahmadov et al., 2007)

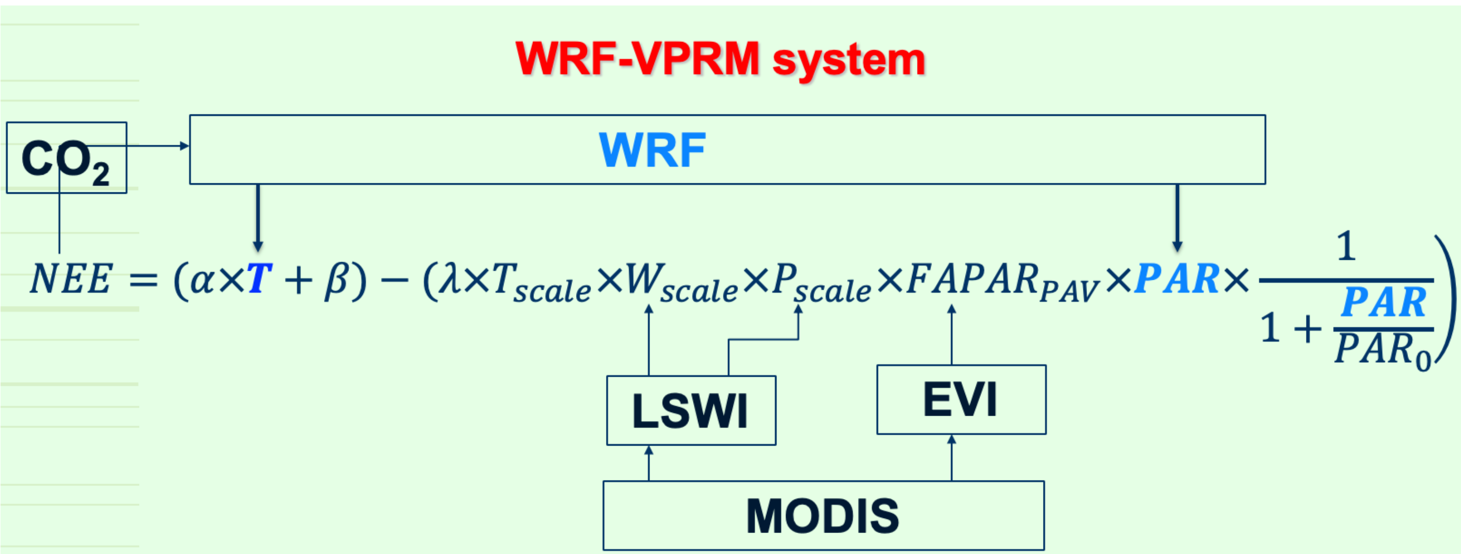

$$NEE = (\alpha \times \boldsymbol{T} + \beta) - \left(\lambda \times T_{scale} \times W_{scale} \times P_{scale} \times FAPAR_{PAV} \times \boldsymbol{PAR} \times \frac{1}{1 + \frac{\boldsymbol{PAR}}{PAR_0}}\right)$$

α, β, λ, PAR_0 need flux data calibration

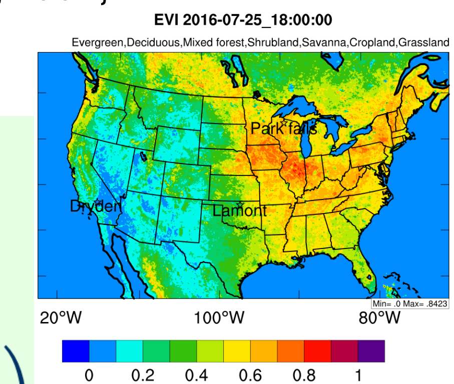

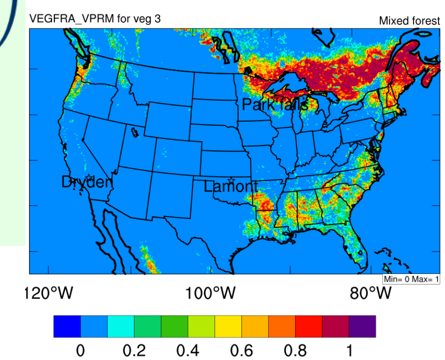

More details in Hu et al., 2020, JAMES

Implemented parameters from Hilton et al. (2013)

Calibrated using eddy covariance tower data over North America

	Evergreen forest	Deciduous forest	Mixed forest	Shrub	Savanna	Crop	Grass
PAR_0	745.306	514.13	419.5	590.7	600	1074.9	717.1
λ	0.13	0.1	0.1	0.18	0.18	0.085	0.115
α	0.1247	0.092	0.2	0.0634	0.2	0.13	0.0515
β	0.2496	0.843	0.27248	0.2684	0.3376	0.542	-0.0986

And other minor changes to VPRM in WRF

Downscaling in 2016 from CarbonTracker

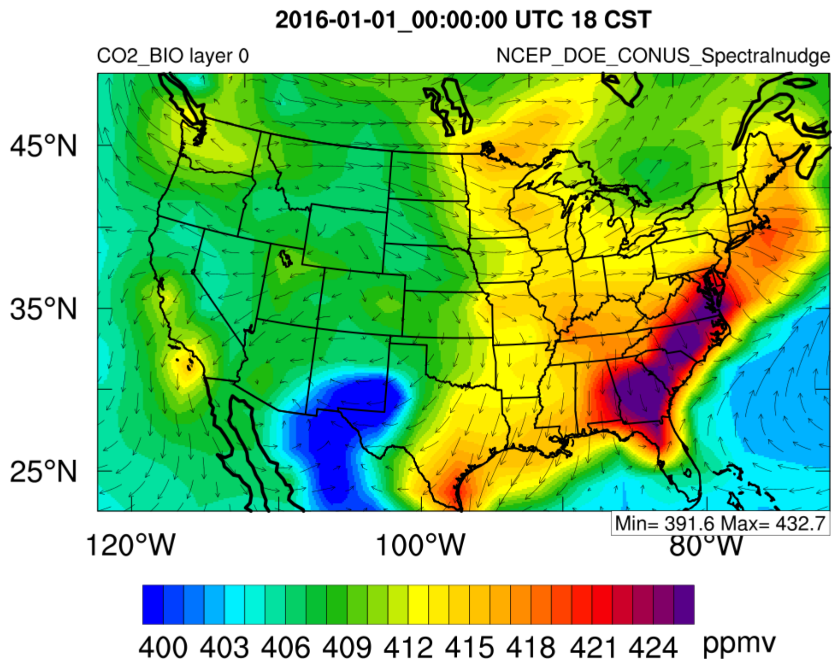

WRF-VPRM IC

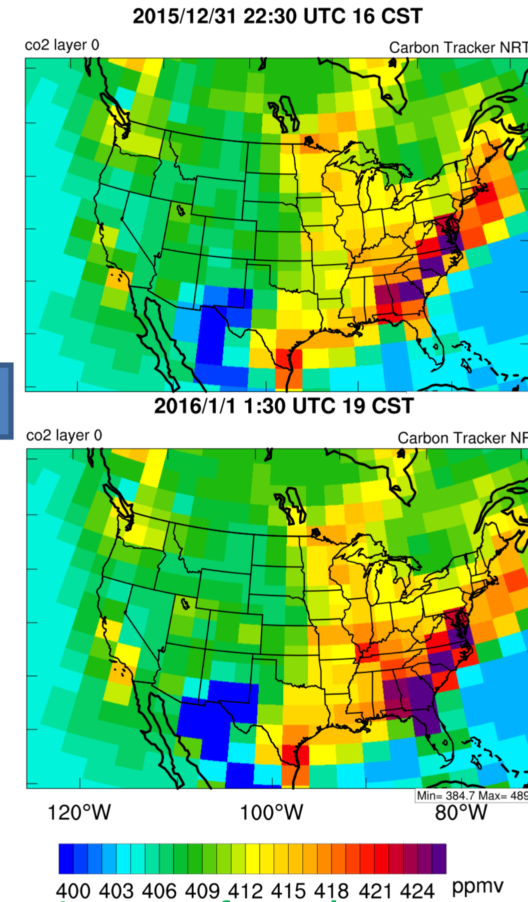

Point 1: both IC/BC are time dependent

Point 2: resolution of WRF-VPRM is much higher, adequate to investigate impact of weather

configuration for WRF-VPRM downscaling

Short wave radiation	Dudhia
Long wave radiation	rapid radiative transfer model (RRTM)
Boundary layer	YSU
Microphysics	Morrison
Cumulus	Grell-Freitas
Land surface model	NOAH
Vertical levels	47
Horizontal resolution	12 km × 12 km with 266×443 grid points
Time step	60 seconds
Meteo initial and lateral boundary conditions	NCEP/DOE Reanalysis 2 (R2)
CO_2 initial and lateral boundary conditions	**CarbonTracker** global simulation $3^o \times 2^o$ outputs
Interior nudging	**Spectral nudging**
nudging variables	horizontal wind components, temperature, geopotential
nudging coefficient	3×10^{-5} s^{-1}
nudging height	above PBL
wave number	5 and 3 in the zonal and meridional directions respectively
nudging period	throughout the downscaling simulation

Biogenic CO_2 fluxes downscaled by WRF-VPRM vs. CarbonTracker posterior fluxes

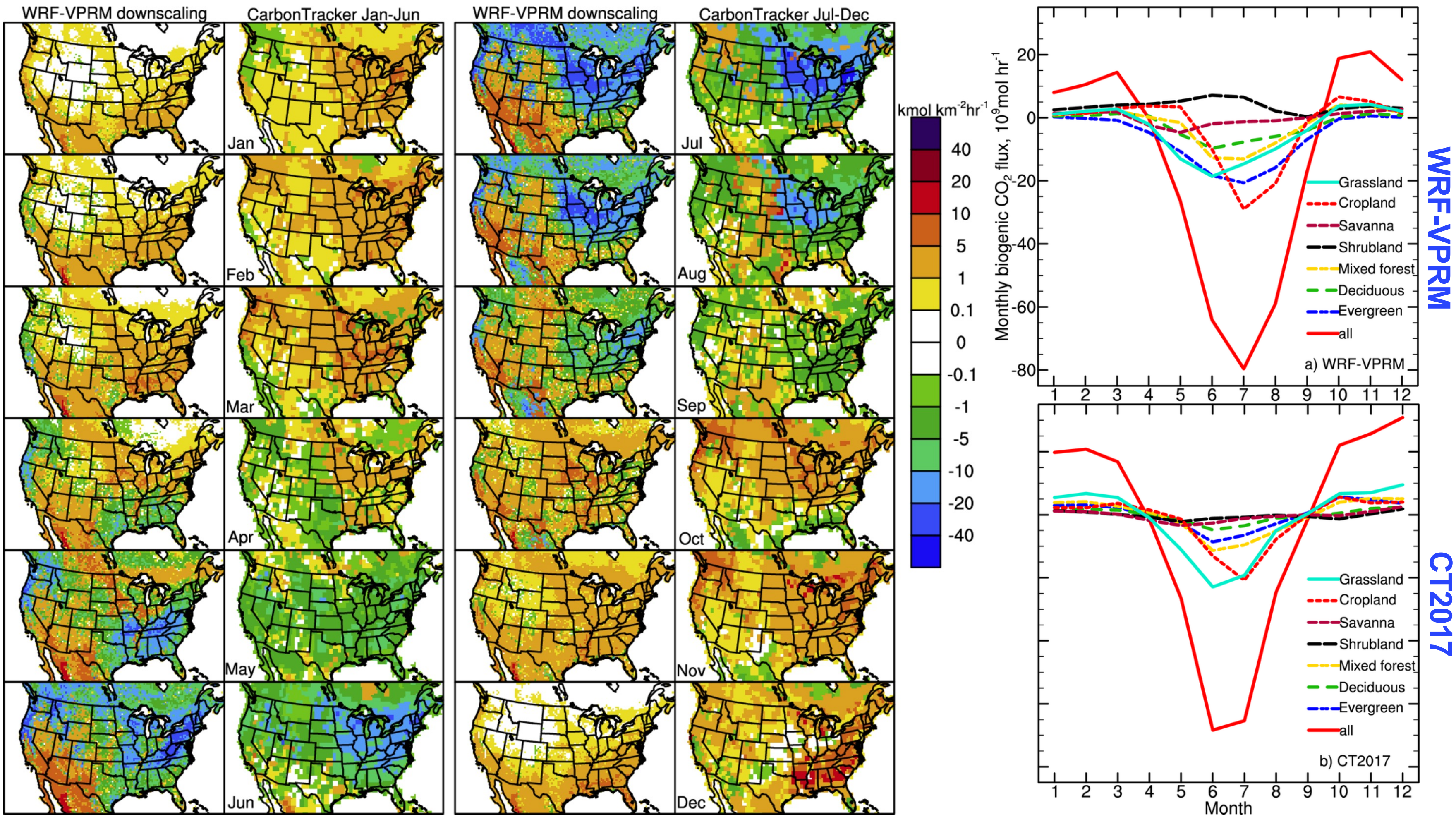

XCO_2 at the 4 TCCON sites

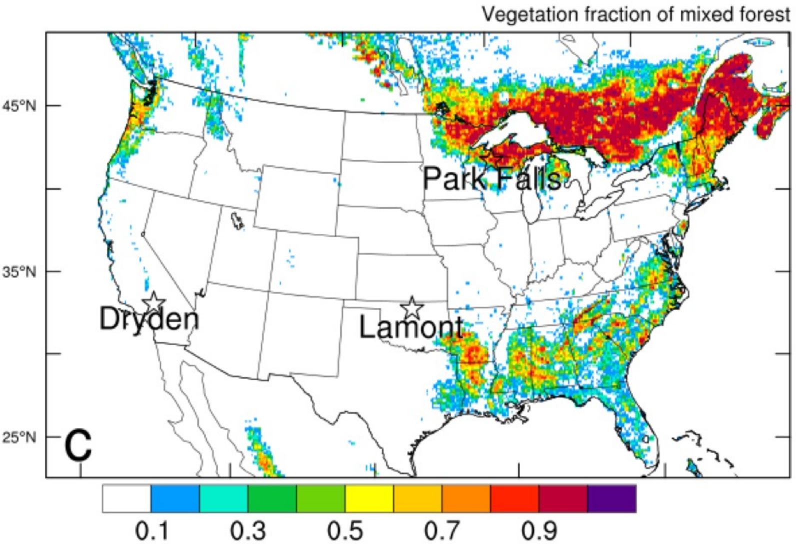

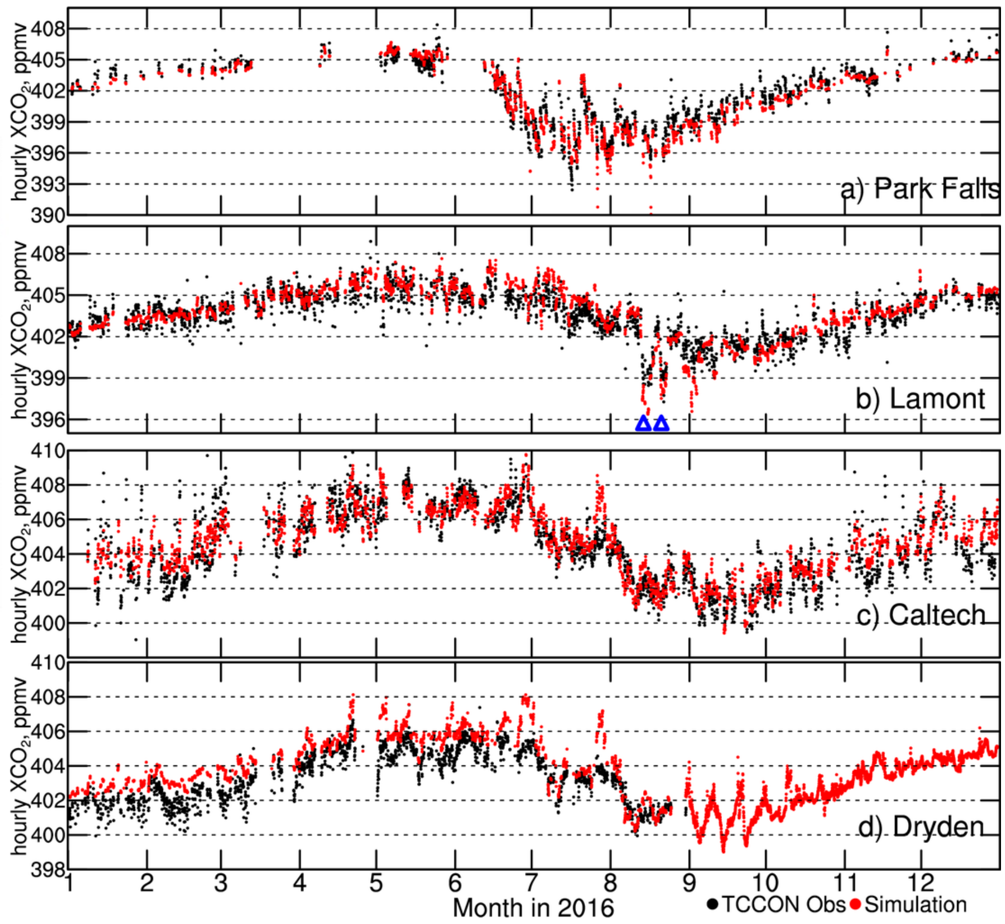

Bias in western boundary?
Bias in anthropogenic emission?

captures the seasonal and some episodic variation of XCO_2.

Evaluation of CT2017

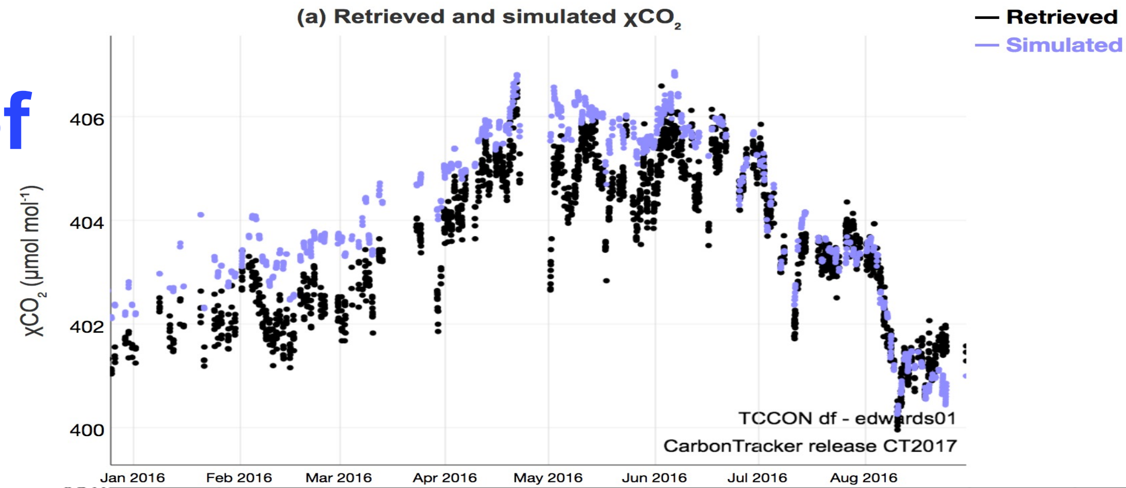

Evaluation of WRF-VPRM

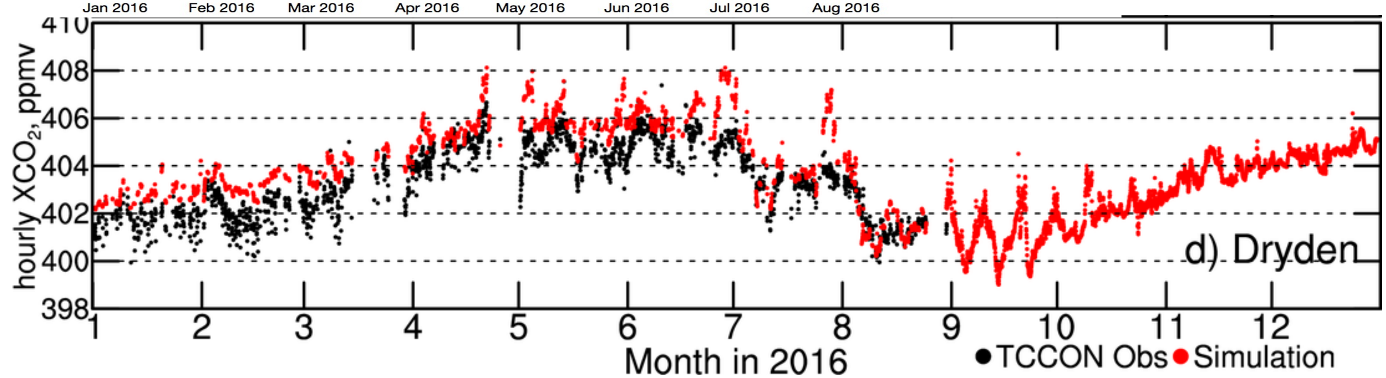

Thus, bias in western boundary partially contributed to WRF-VPRM bias?

Compare with OCO-2; individual contributions

Total

Background

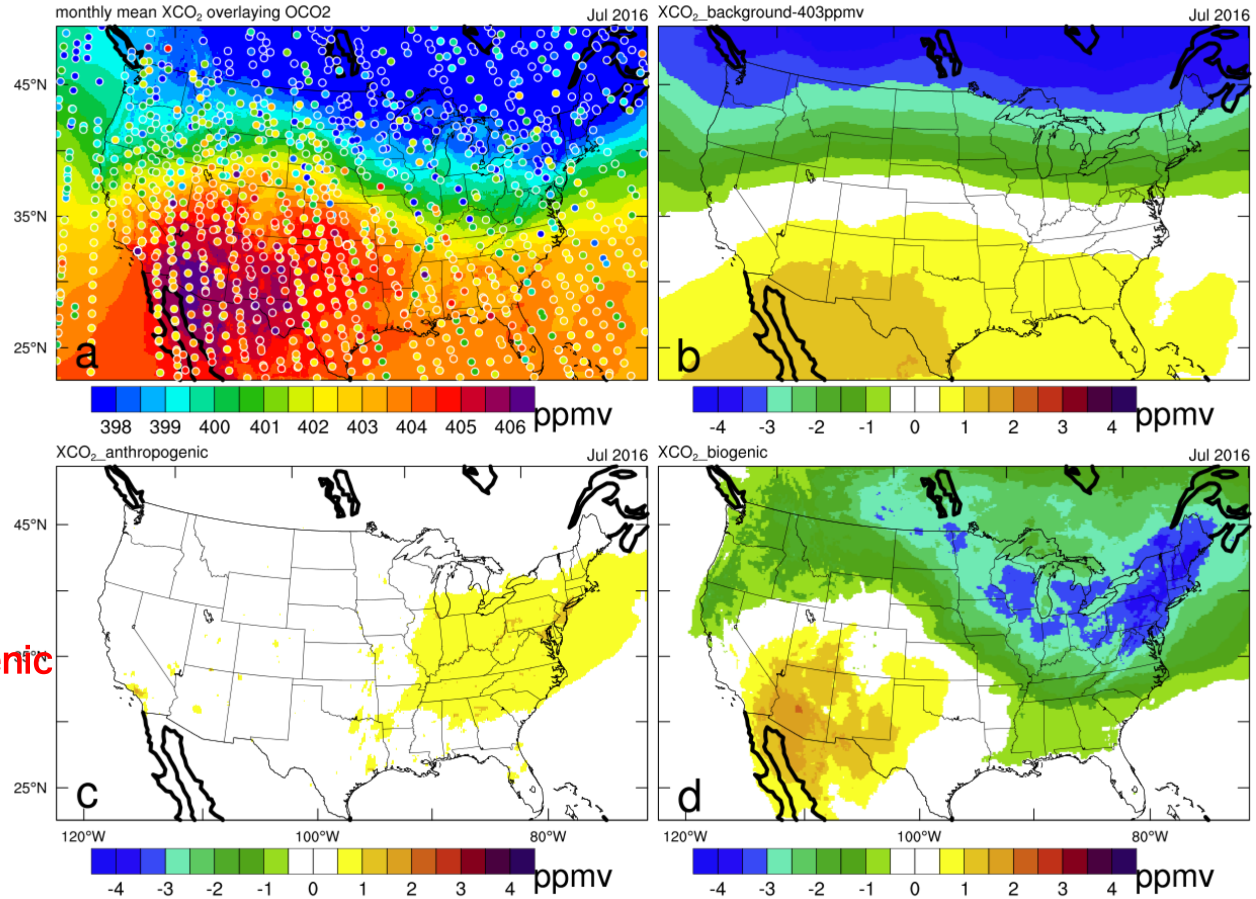

Anthropogenic

Biogenic

Compare with OCO-2, individual cases

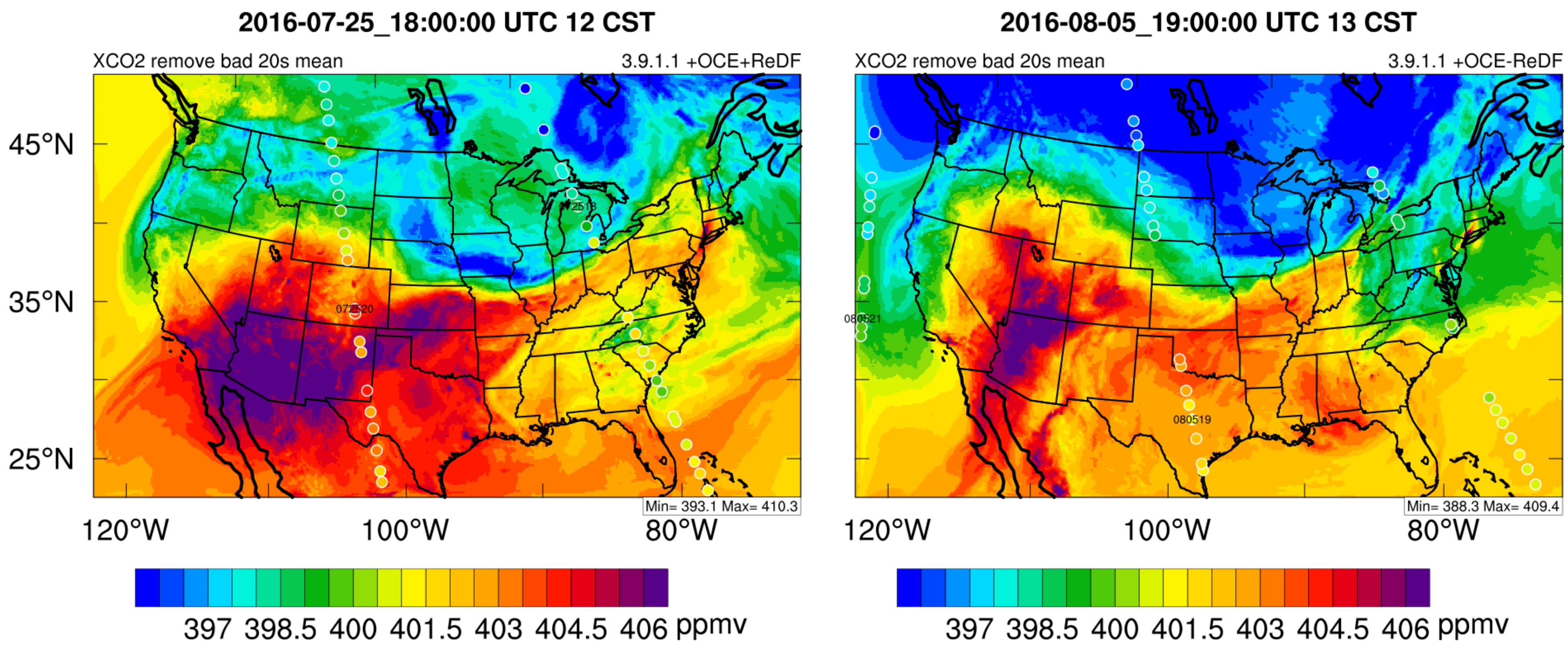

Case study, Aug 5
OCO-2 underpass

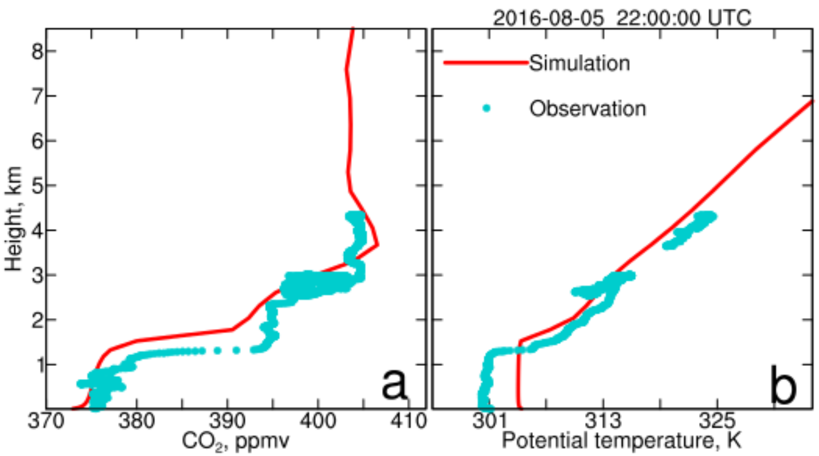

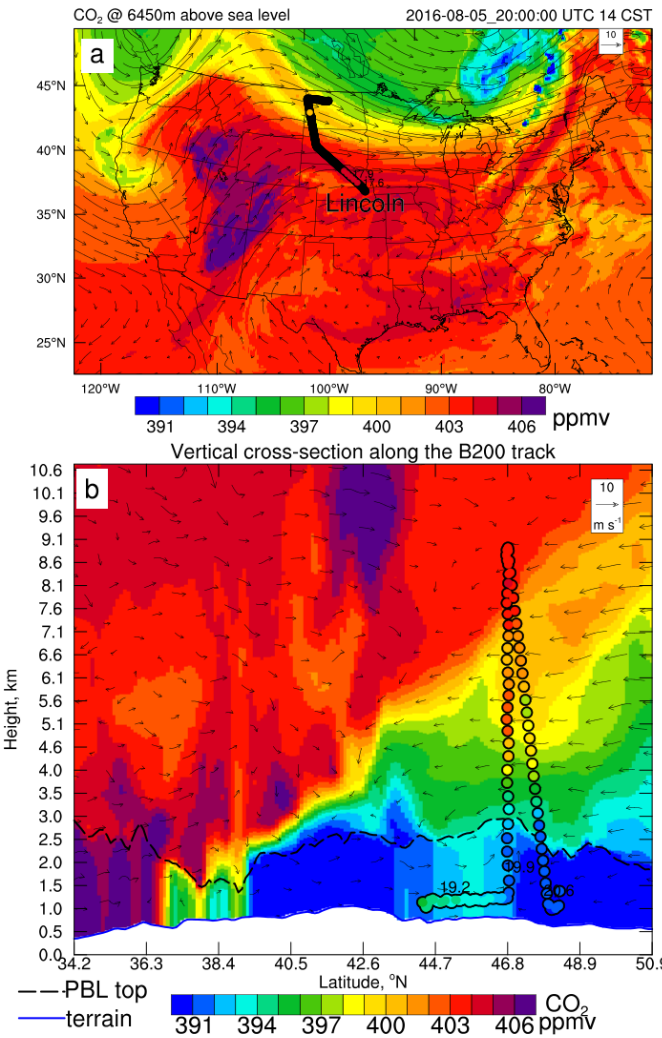

Summary

1. Calibrated VPRM parameters from Hilton et al [2013] are implemented into WRF-VPRM
2. WRF-VPRM reasonably captures monthly variation of XCO_2 and episodic variations due to frontal passages
3. The downscaling also successfully captures the horizontal CO_2 gradients across fronts, as well as vertical CO_2 contrast across the boundary layer top.

Terrestrial CO_2 fluxes in different regions

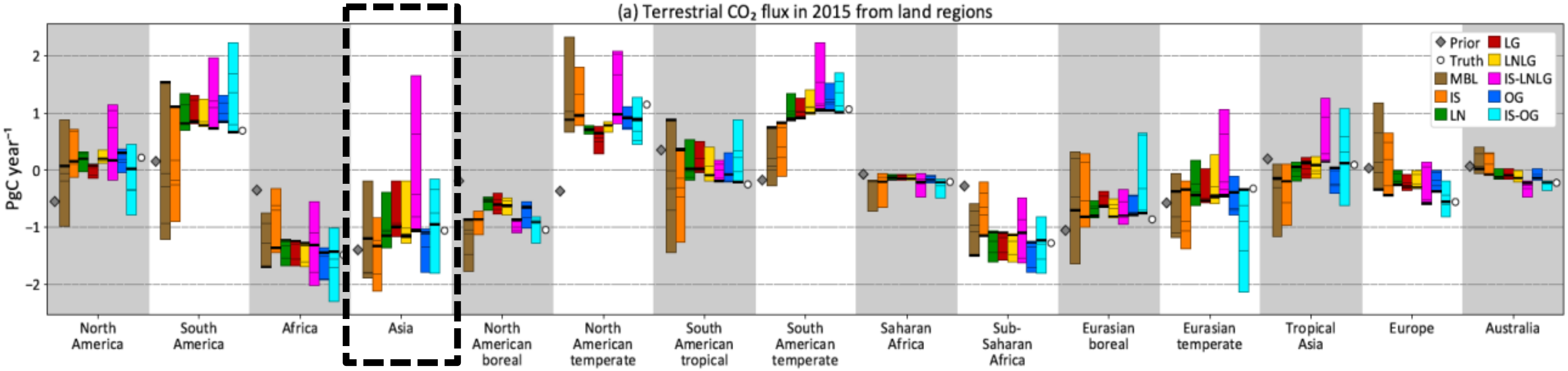

(Sourish Basu et al., 2018)

Uncertainties in each region are large too
Asia is CO_2 sink!!

Northeast China: a major CO_2 sink

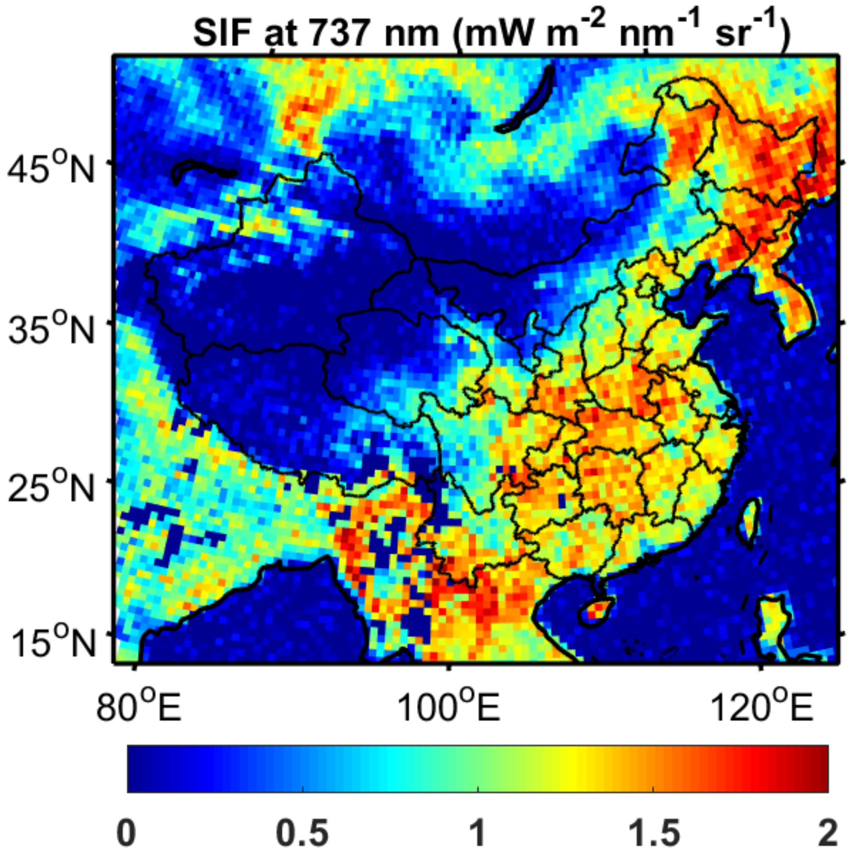

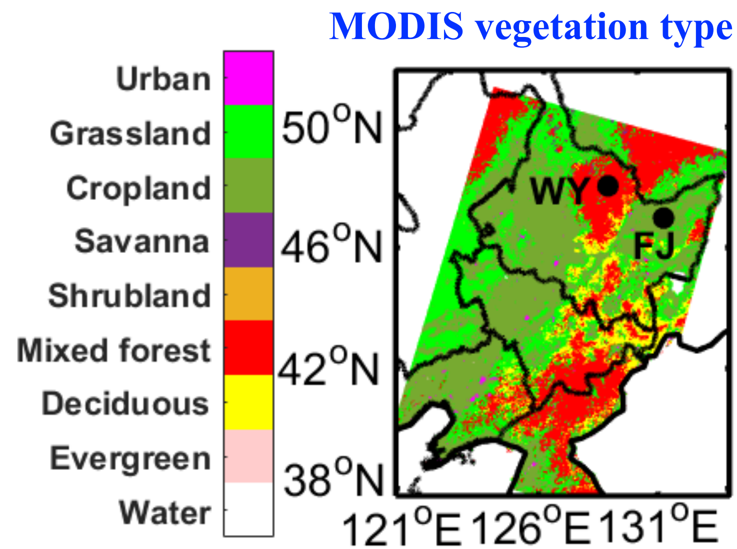

Mixed forest and cropland dominate in Northeast China
Crop area is still increasing!!

SIF: Sun-induced Fluorescence, proportional to photosynthesis

Long-term tower measurements, focusing on 2016

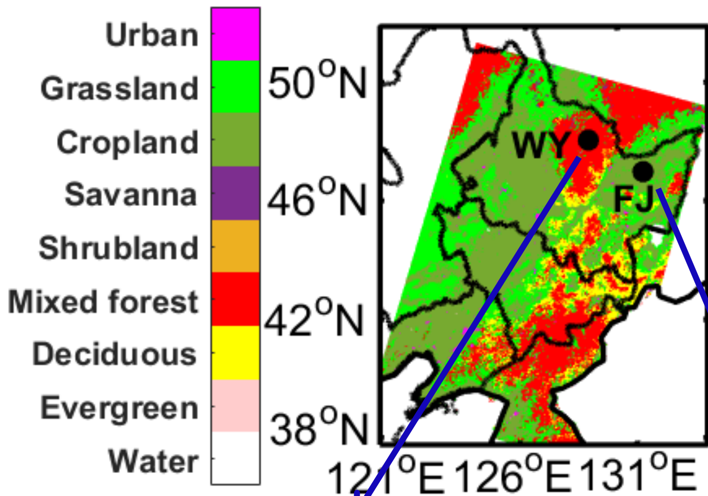

- **Observational parameters:**
  1) Hourly mean CO_2 fluxes and concentrations,
  2) wind speed and direction, air temperature
  3) PAR (only at Fujin)

- **Observational period:**
  Fujin: since 2012
  Wuying: since 2014

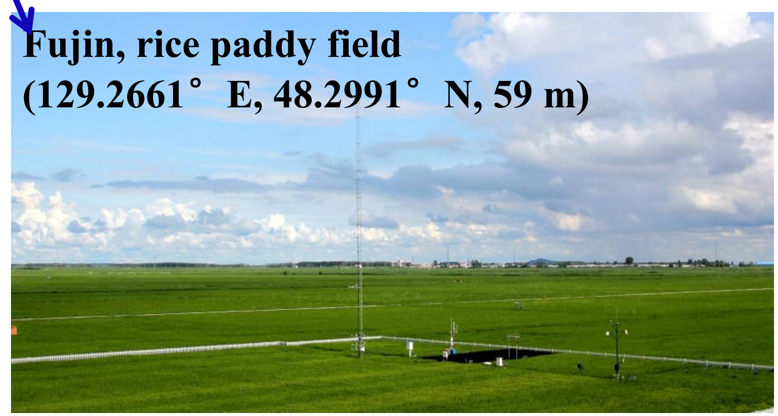

Seasonal variations of CO_2 fluxes and concentrations

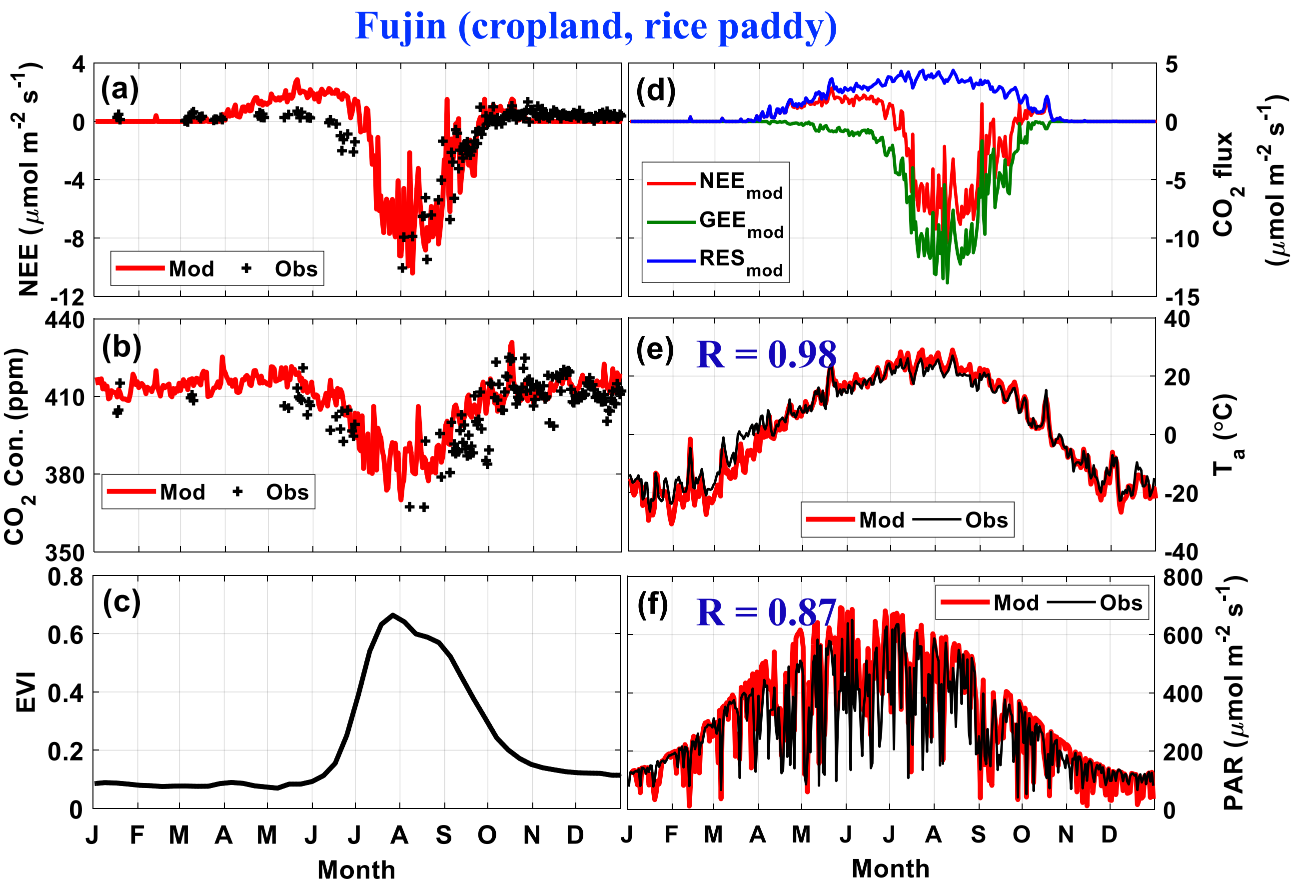

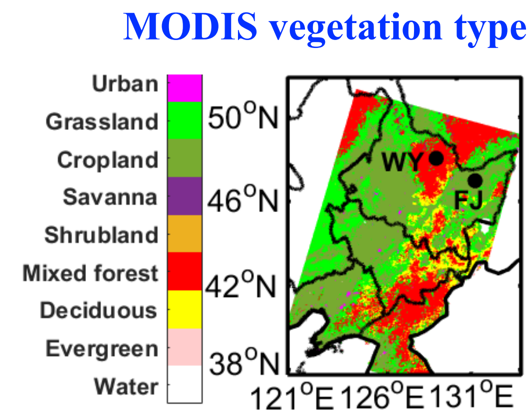

Bias of terrestrial respiration

Fujin (cropland, rice paddy)

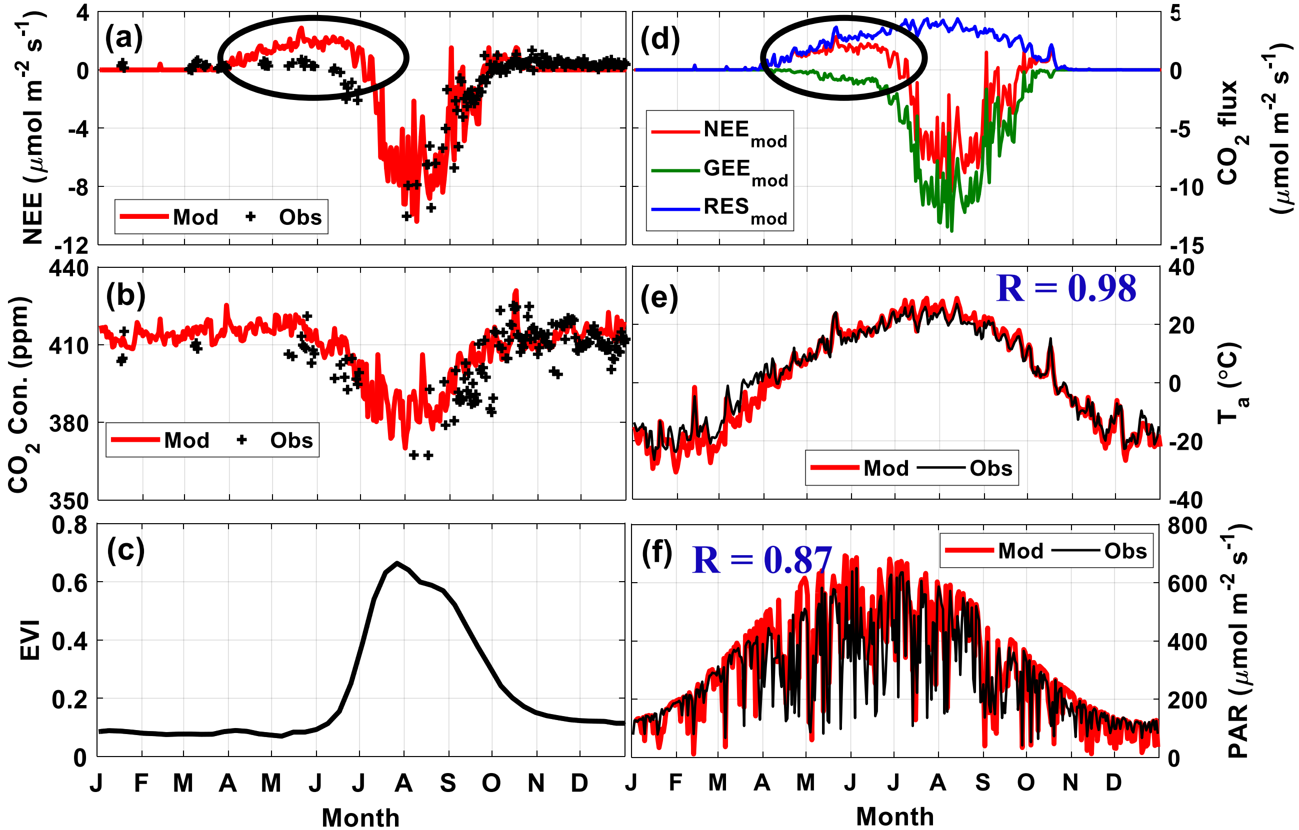

$$NEE = (\alpha \times T + \beta) + GEE$$

largely subjected to the EVI

Ignores leaf mass, involves EVI?

Seasonal variation of CO_2 fluxes and concentrations

Wuying (mixed forest)

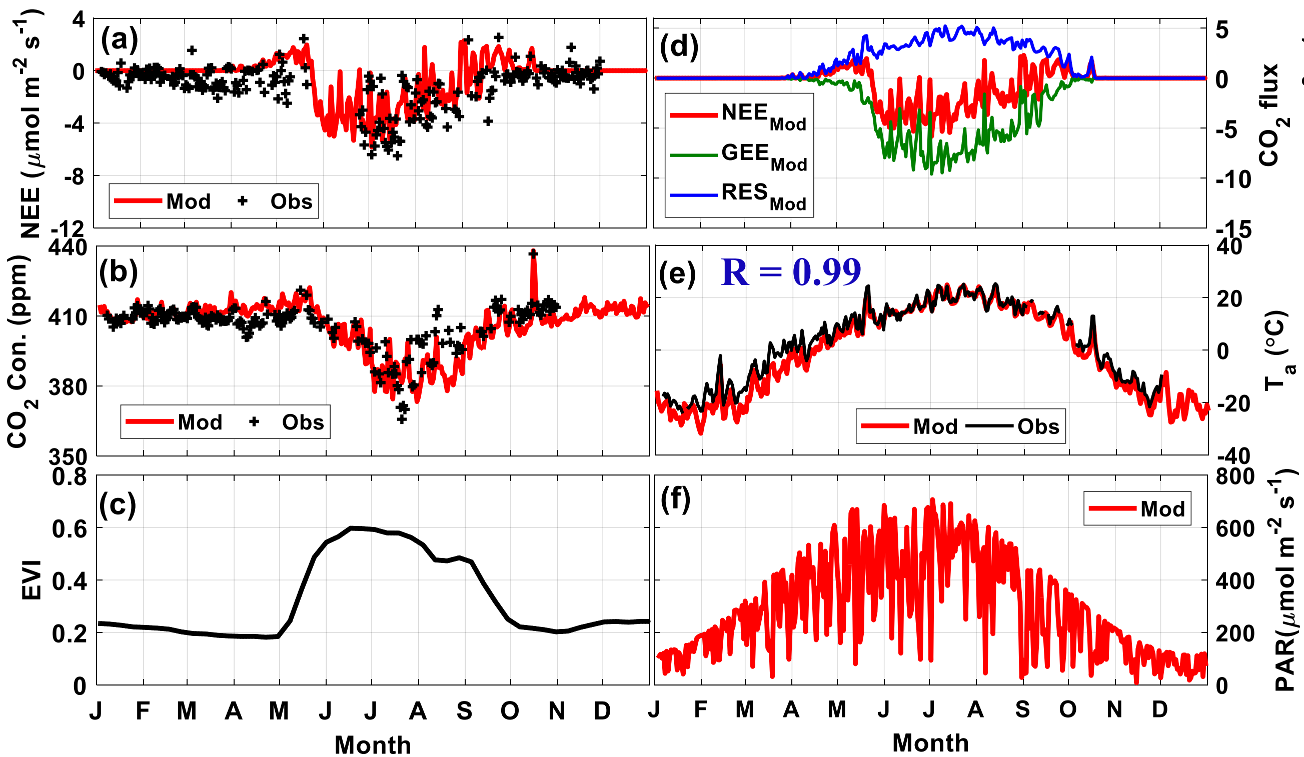

MODIS vegetation type

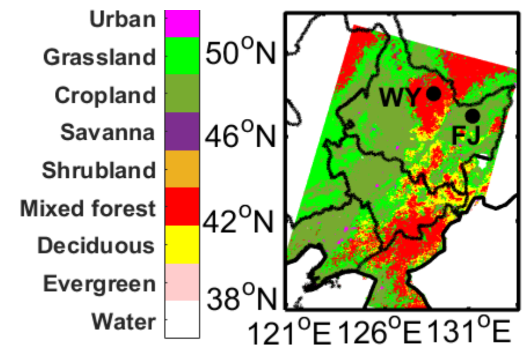

OCO-2 retrieved XCO_2 (L2 Lite Version 9)

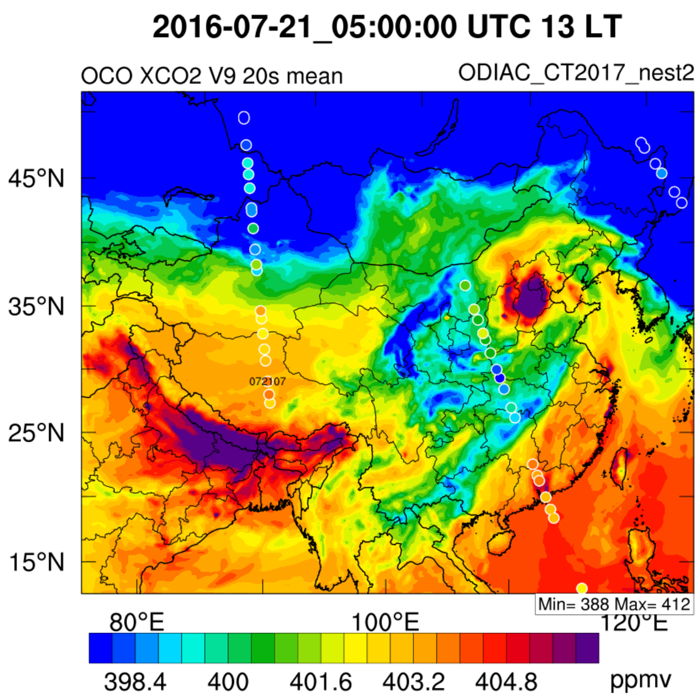

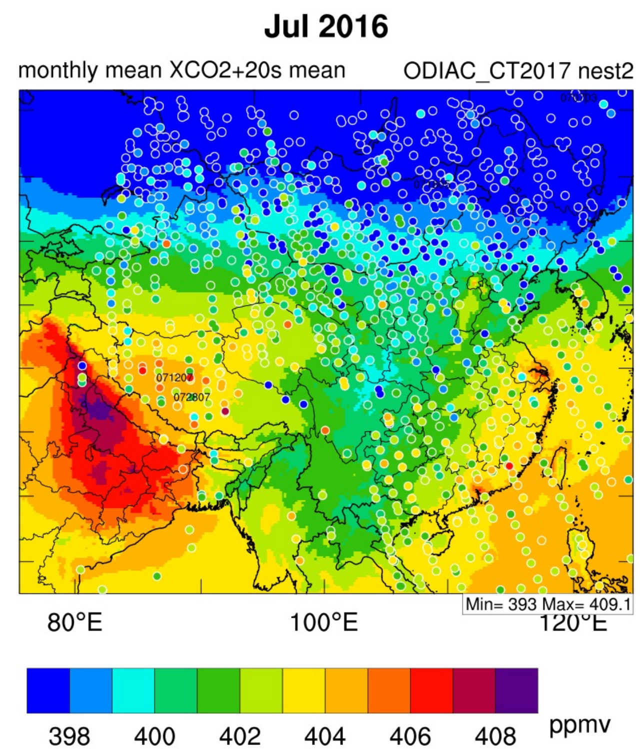

Advantage: spatiotemporal coverage
Disadvantage: interfere with cloud and haze pollution!!

Seasonal variation of XCO_2 over Northeast China

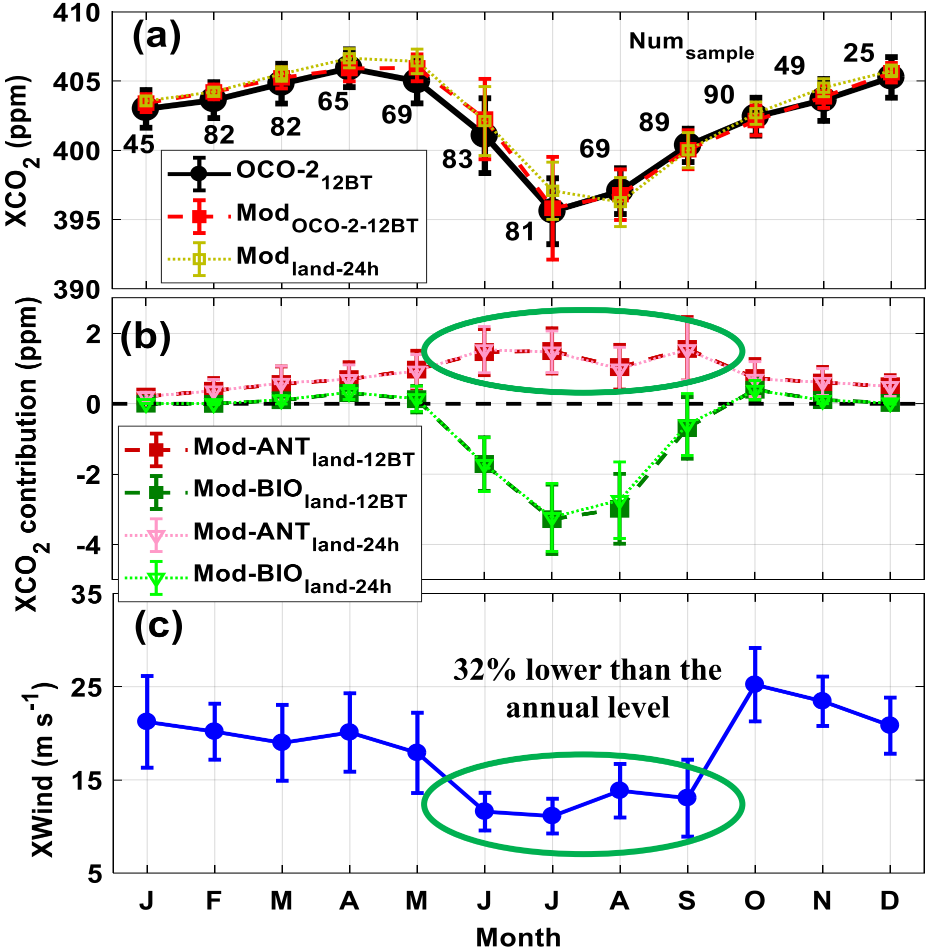

Seasonal variation range: 10 ppmv

Annual mean contribution:

- anthropogenic: 0.84 ppmv
- biogenic: -0.60 ppmv

Weak winds favors the large anthropogenic contribution of XCO_2 in summer

Mean diurnal variation of CO_2 fluxes and concentrations in growing season

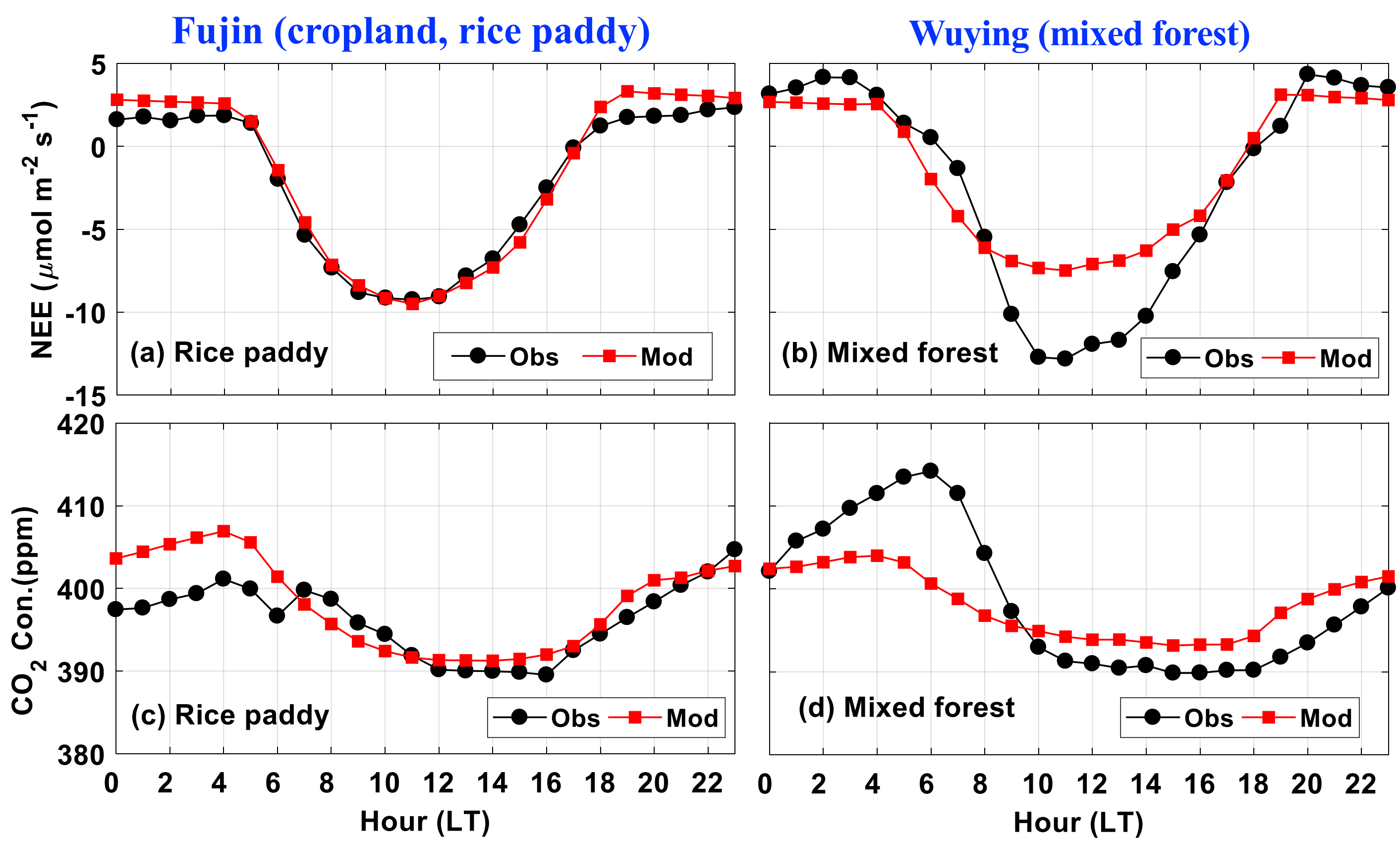

WRF-VPRM underestimates diurnal variation range over mixed forest

Conclusions and future work

- **Mixed forest is observed as a stronger CO_2 sink/source than rice paddy on average in 2016;**
- **Negative biogenic contribution offset about 70% of anthropogenic contribution of XCO_2 over Northeast China in 2016;**
- **The uncertainty of NEE simulation largely depends on four VPRM parameters, especially the maximum light use efficiency λ.**

Further improvement of WRF-VPRM
Updated CO_2 flux parameterization

$$\mathrm{ER} = \alpha \times T + \beta$$

(Gourdji et al., 2020):

$$ER = \beta + \alpha_1 \cdot T + \alpha_2 \cdot T^2 + \gamma \cdot EVI + k_1 \cdot W_{scale} + k_2 \cdot W_{scale} \cdot T + k_3 \cdot W_{scale} \cdot T^2$$

incorporating EVI, water stress scaling factor (W_{scale}), and a quadratic dependence on Tair

More details in Hu et al., 2021, JGR

CO_2 flux evaluation

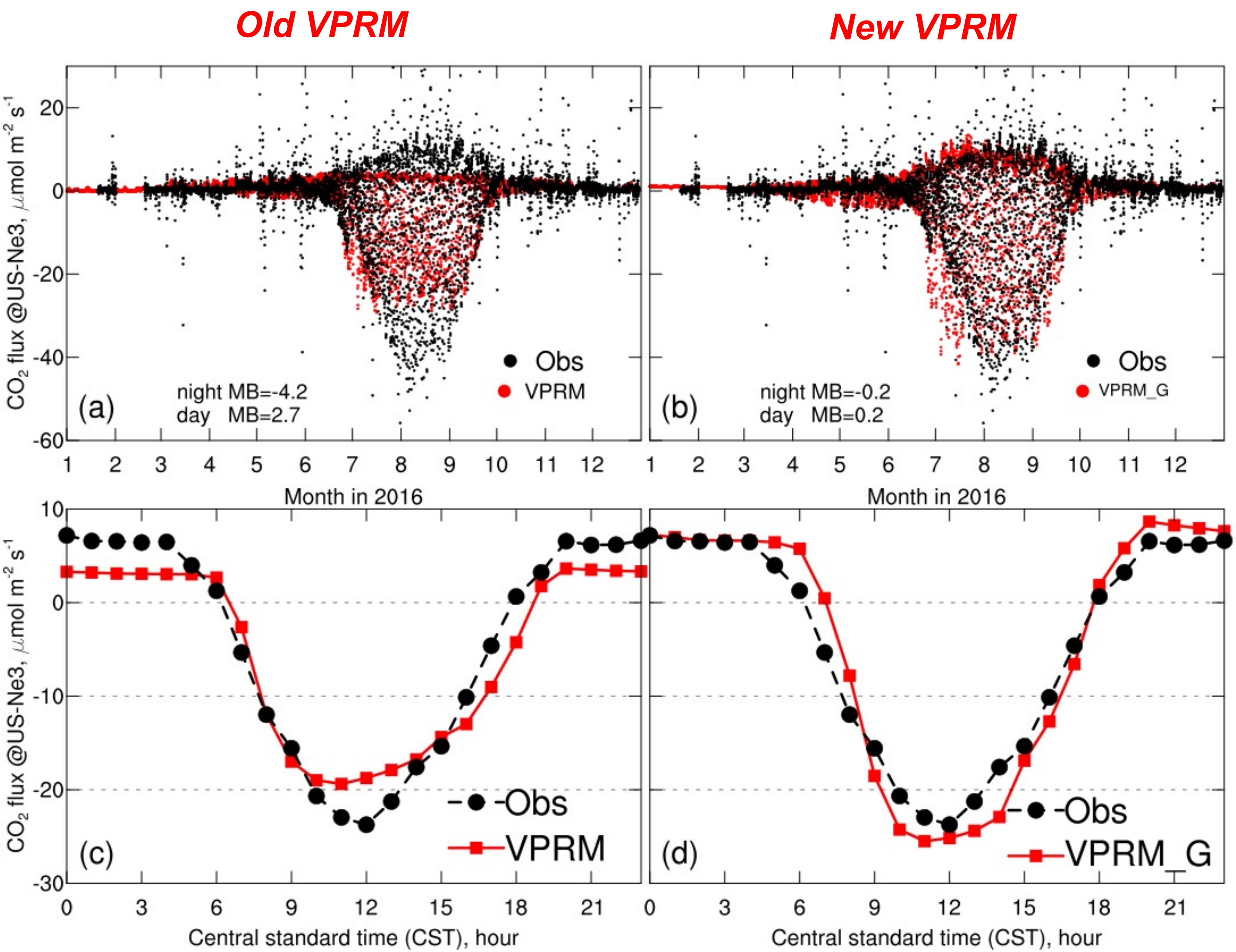

Evaluation data: NOAA towers

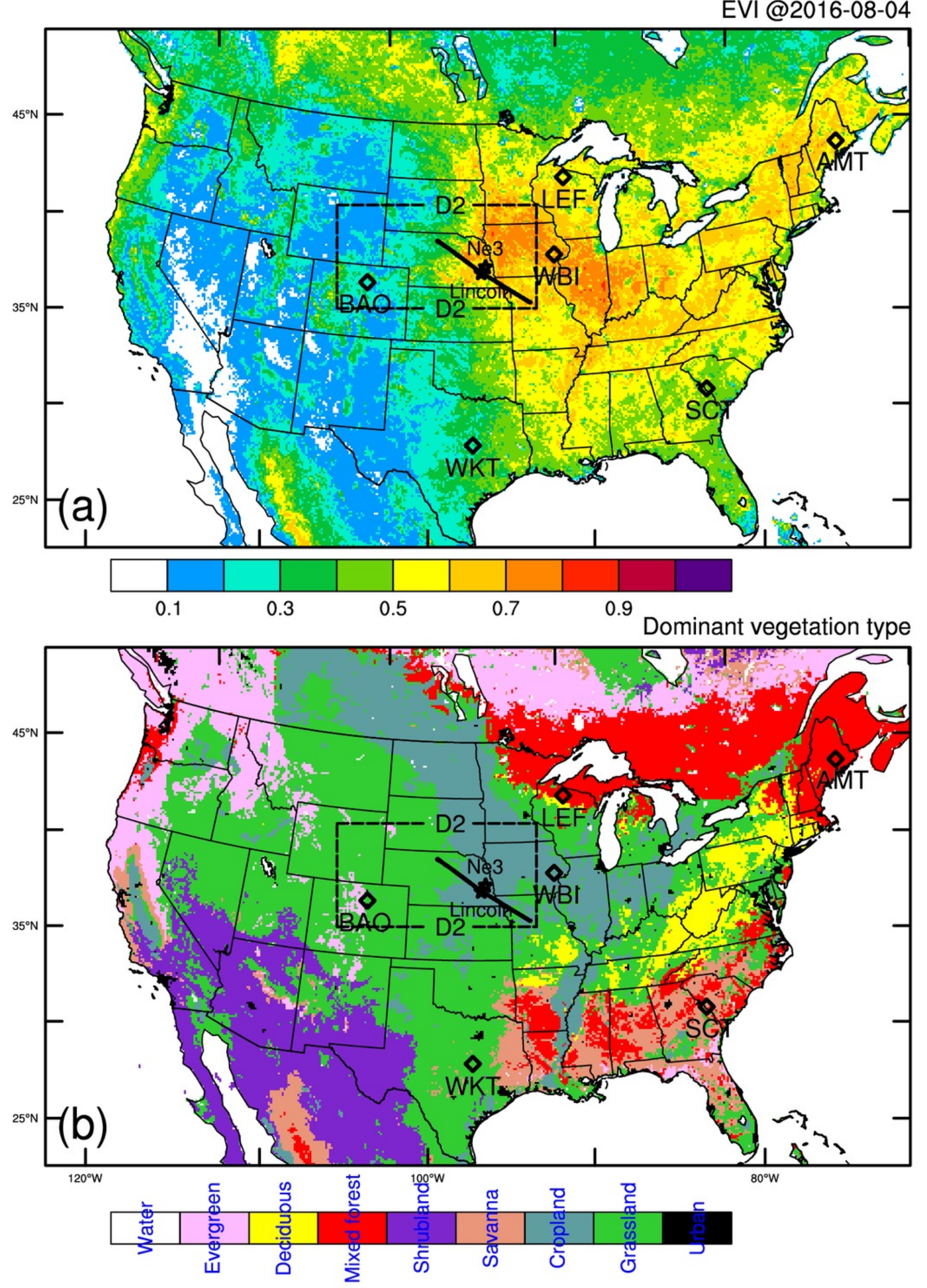

CO_2 concentration evaluation

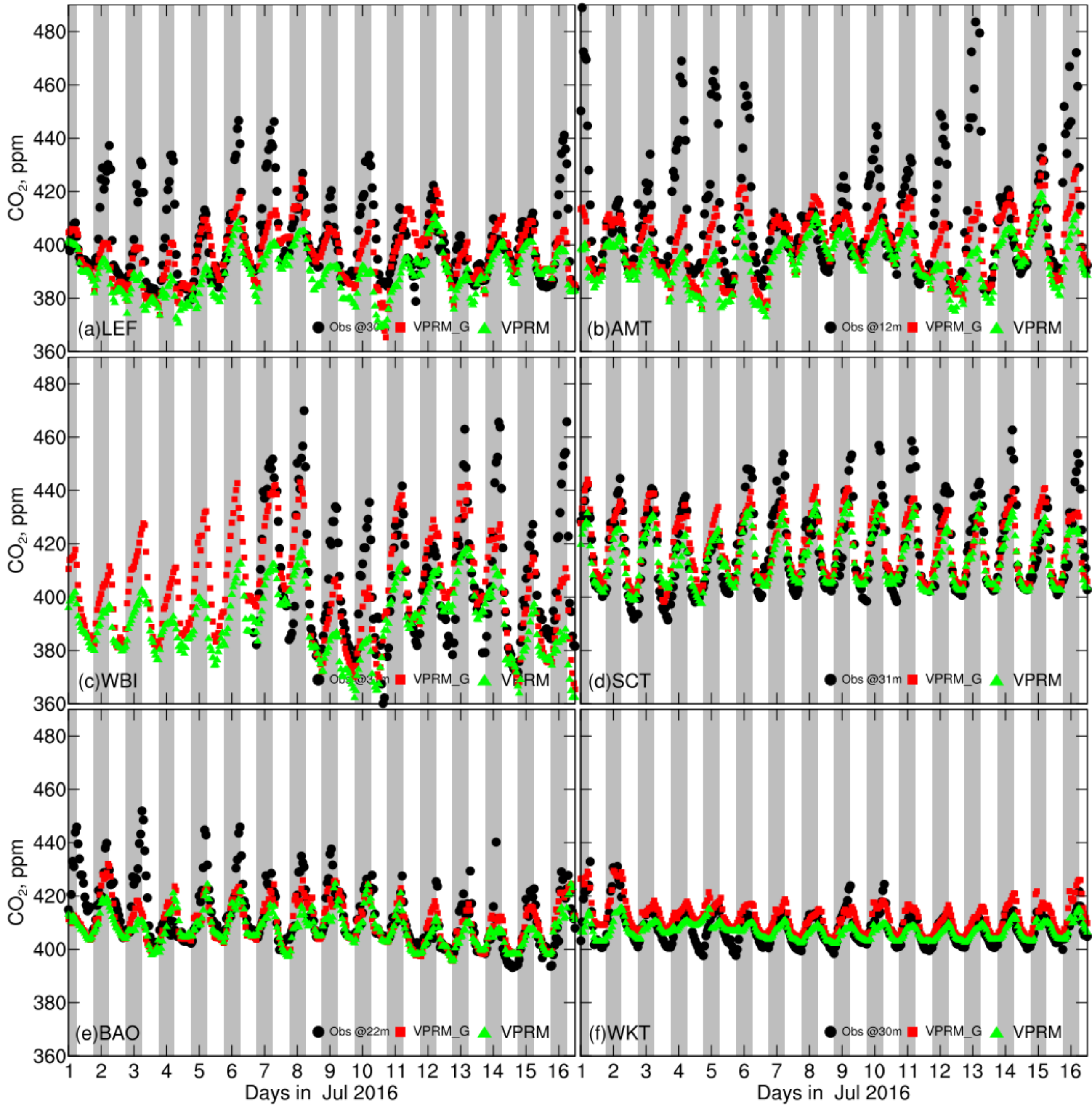

Using new VPRM to examine CO_2 band

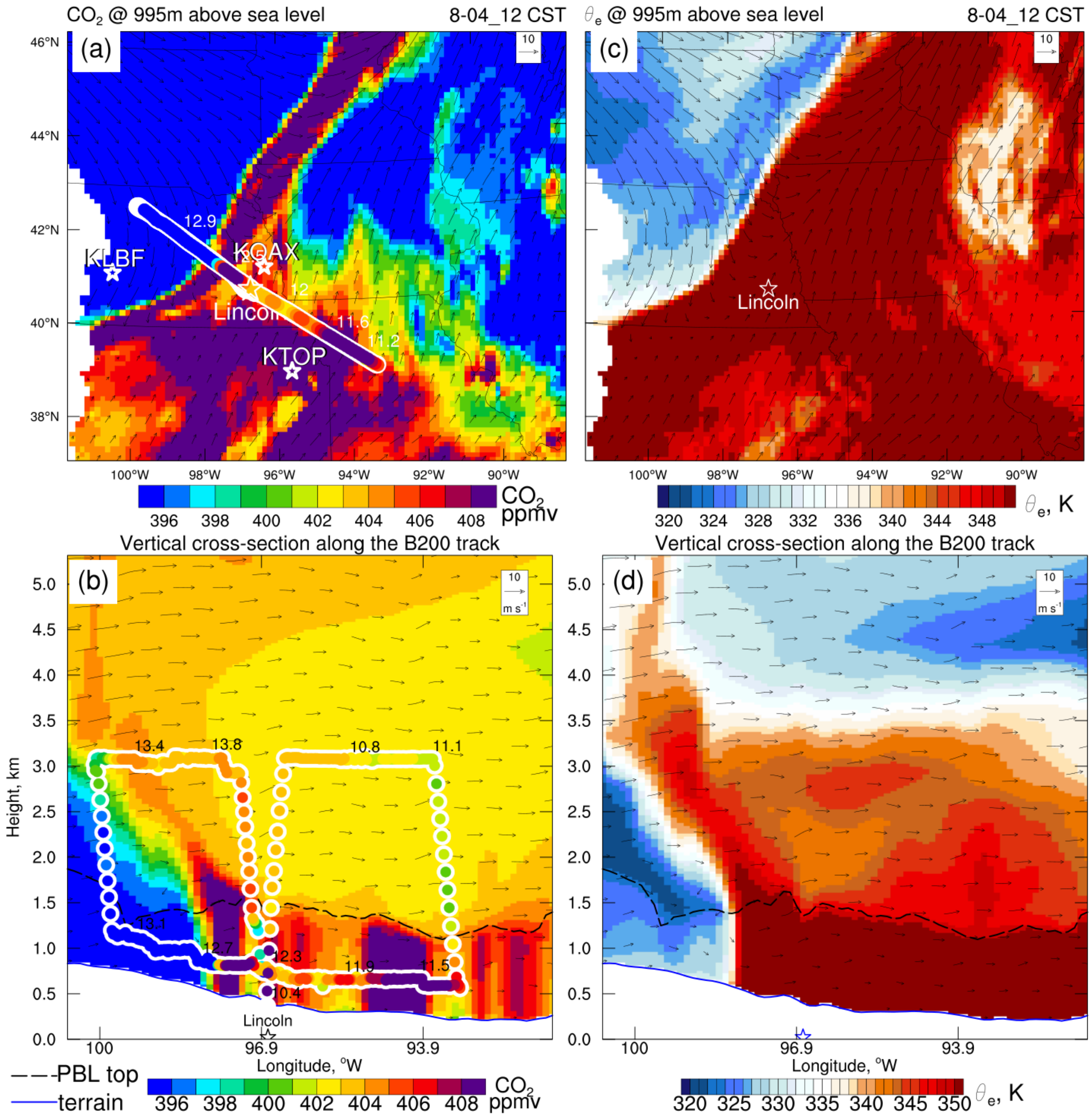

Application of improved WRF-VPRM in China to examine CO_2 flux

Name	Site	Altitude (m)	Substrate
Maqu	33.8975° N, 102.1619° E	3423	Kobresia tibetica and K. humilis
Yakou	38.0142° N, 100.2421° E	4148	Alpine grassland
Dashalong	38.8399° N, 98.9406° E	3739	Swampy alpine meadows
Arou	38.0473° N, 100.4643° E	3033	Alpine grassland
Nam CO	30.7667° N, 90.95° E	4730	K. pygmaea and alpine steppe
Mt. Waliguan	36.28° N, 100.9° E	3810	Arid and semi-arid grasslands, tundra, and deserts

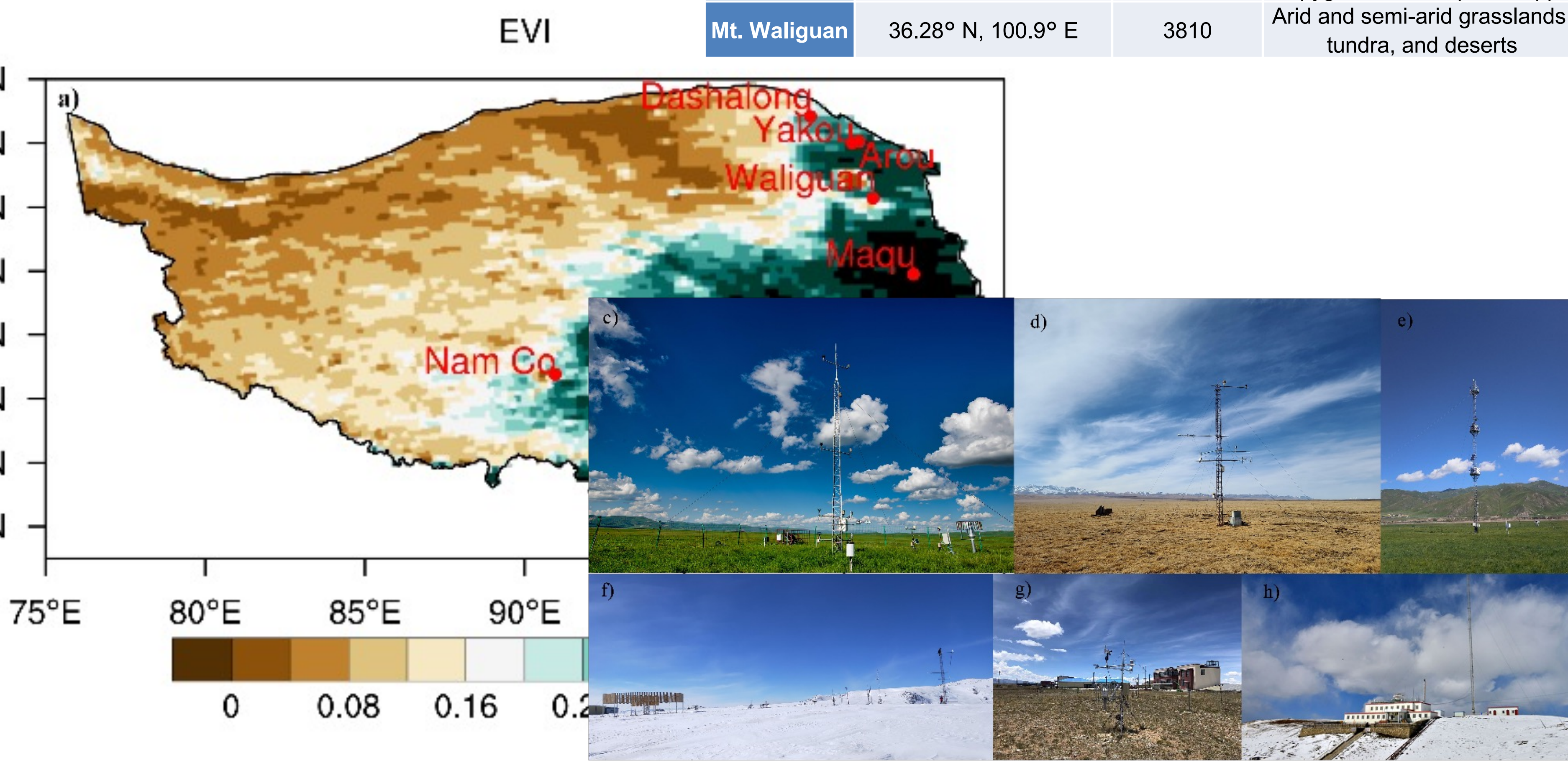

Niu and Hu et al. (2023)

Application of improved WRF-VPRM in China to examine CO_2 flux

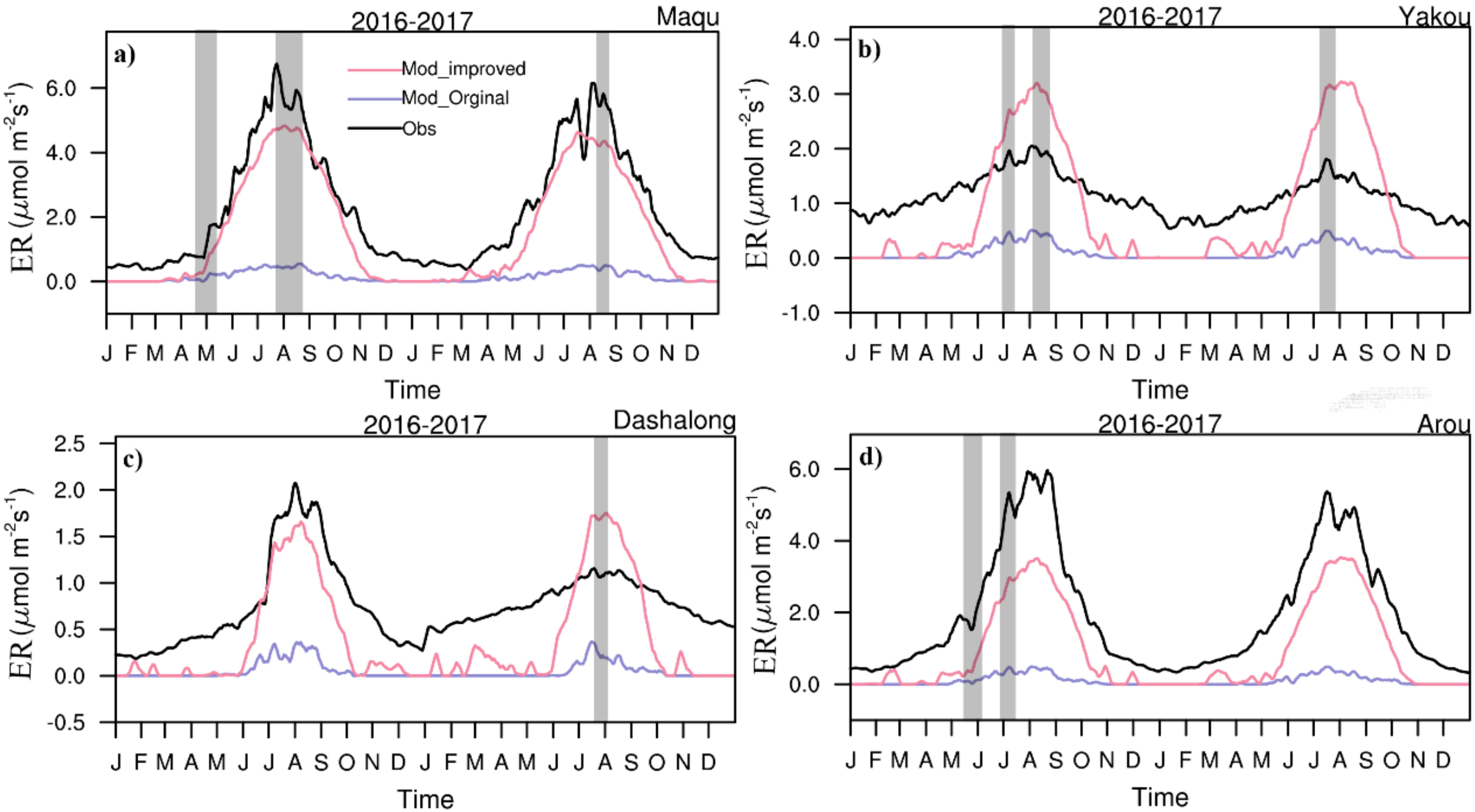

Niu and Hu et al. (2023)

Application of improved WRF-VPRM in China to examine CO_2 flux

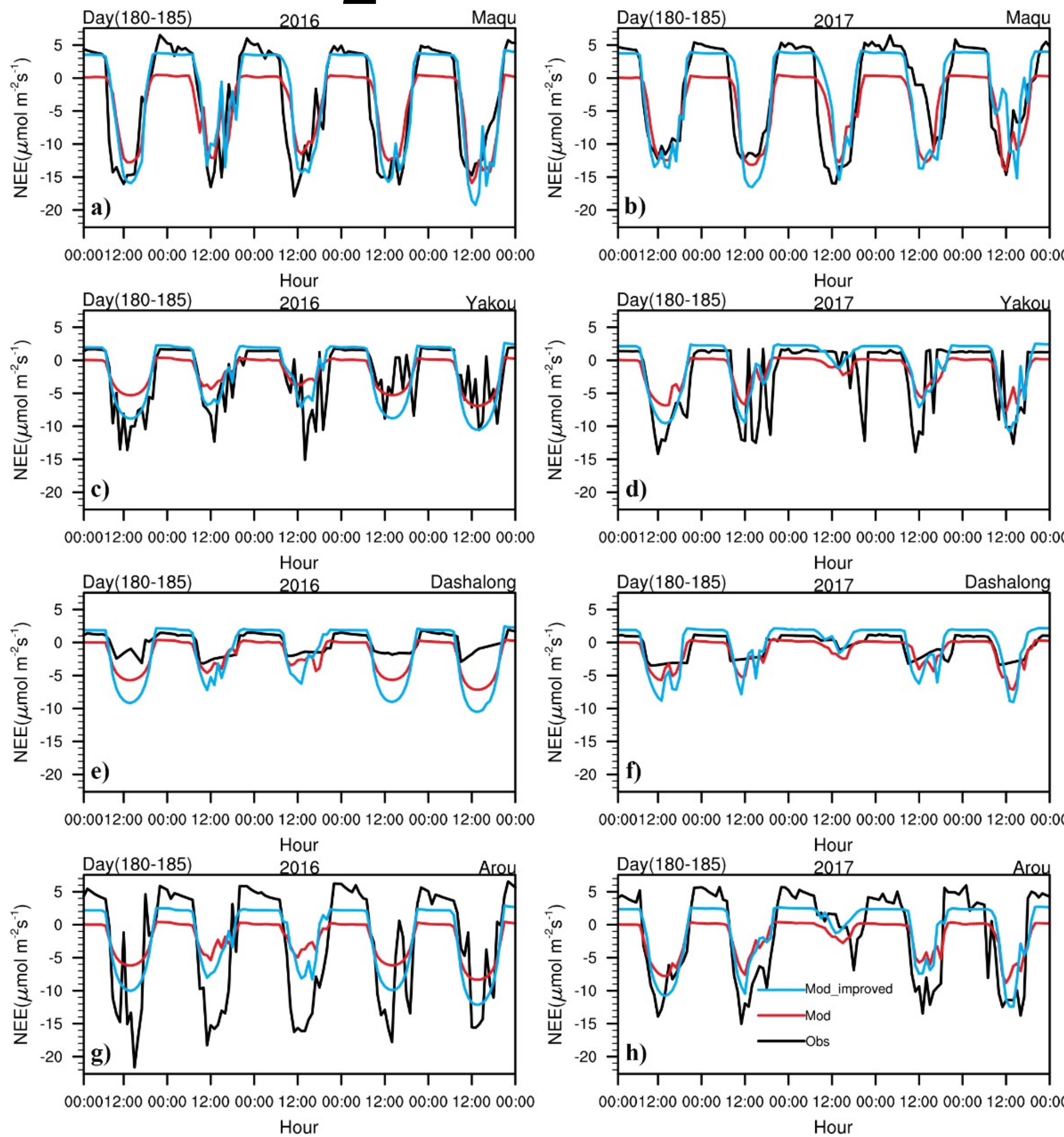

Niu and Hu et al. (2023)

1. 3D WRF-CO2 simulation

Over US and China

2. Multi-Model investigation of Haze Pollution

3. WRF-GHG for both CO_2 and CH_4 simulation

4. CH4 inversion

Haze pollution in China

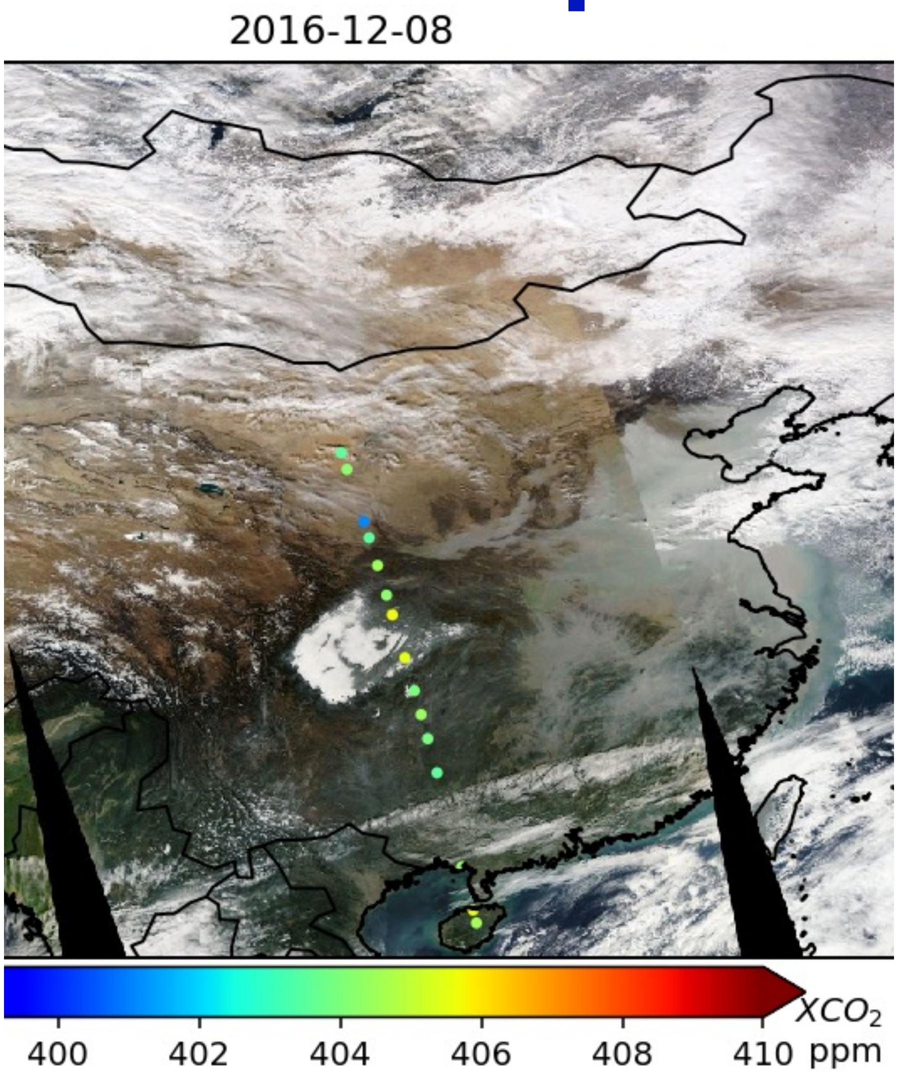

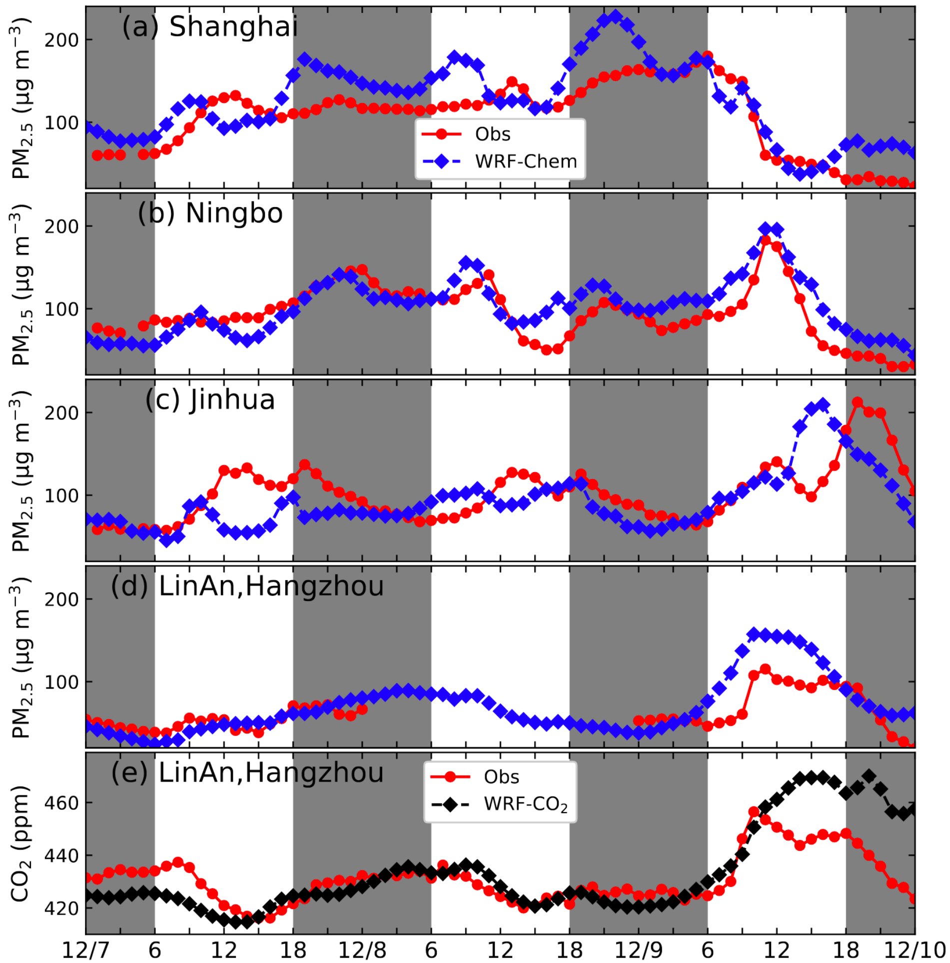

Heaviest haze pollution in China in 2016

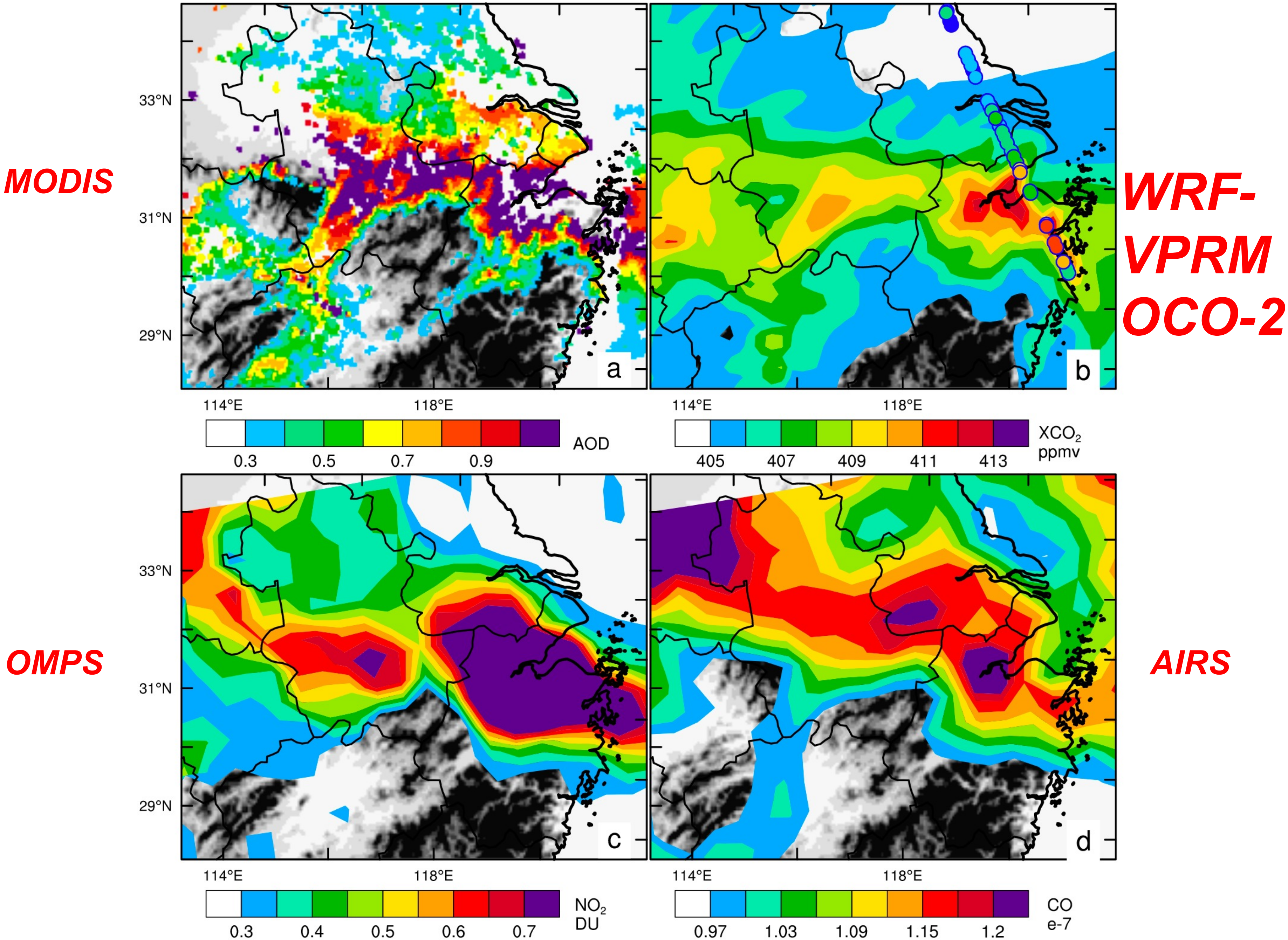

MODIS
WRF-
VPRM
OCO-2
OMPS
AIRS
33°N
31°N
29°N
114°E
118°E
a
b
c
d
AOD
0.3 0.5 0.7 0.9
XCO2 ppmv
405 407 409 411 413
NO2 DU
0.3 0.4 0.5 0.6 0.7
CO e-7
0.97 1.03 1.09 1.15 1.2

Conclusions

1. **A severe haze pollution at the leading edge of a cold front in China on Dec. 9, 2016 is examined using multi-sensors and multi-models, including WRF-Chem and WRF-CO_2.**

2. **Satellite-retrieved column-averaged CO_2 data can be used to monitor air pollution events collectively with other in situ and remote-sensing instruments.**

3. **Channel winds between Mountains Dabie and Huang transport pollutants from the North China Plain and Yangtze River Delta Region to Jiangxi Province**

1. 3D WRF-CO2 simulation

Over US and China

2. Multi-Model investigation of Haze Pollution

3. WRF-GHG for both CO_2 and CH_4 simulation

4. CH4 inversion

WRF-GHG coupled with CAMS

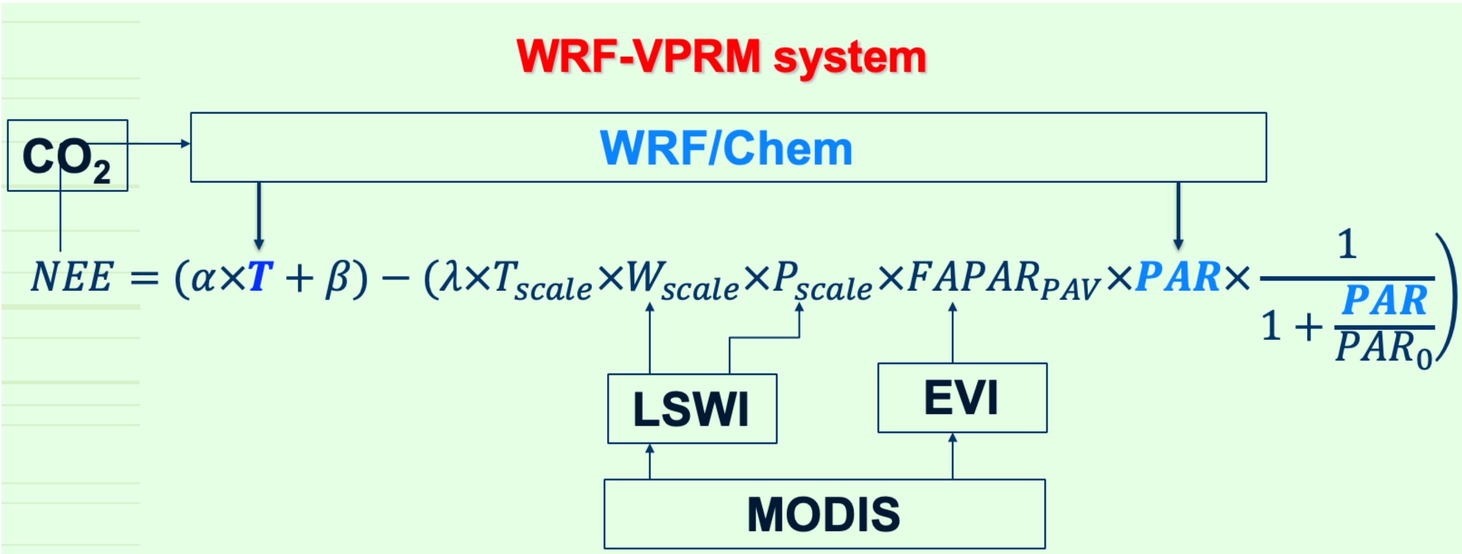

Included CH_4 recently doi/10.1002/essoar.10508159.1

the *WetCHARTs* wetland CH_4 emissions

EPA NEI2017 anthropogenic CH_4 emissions

WRF-GHG simulation vs. TCCON observation

CO_2

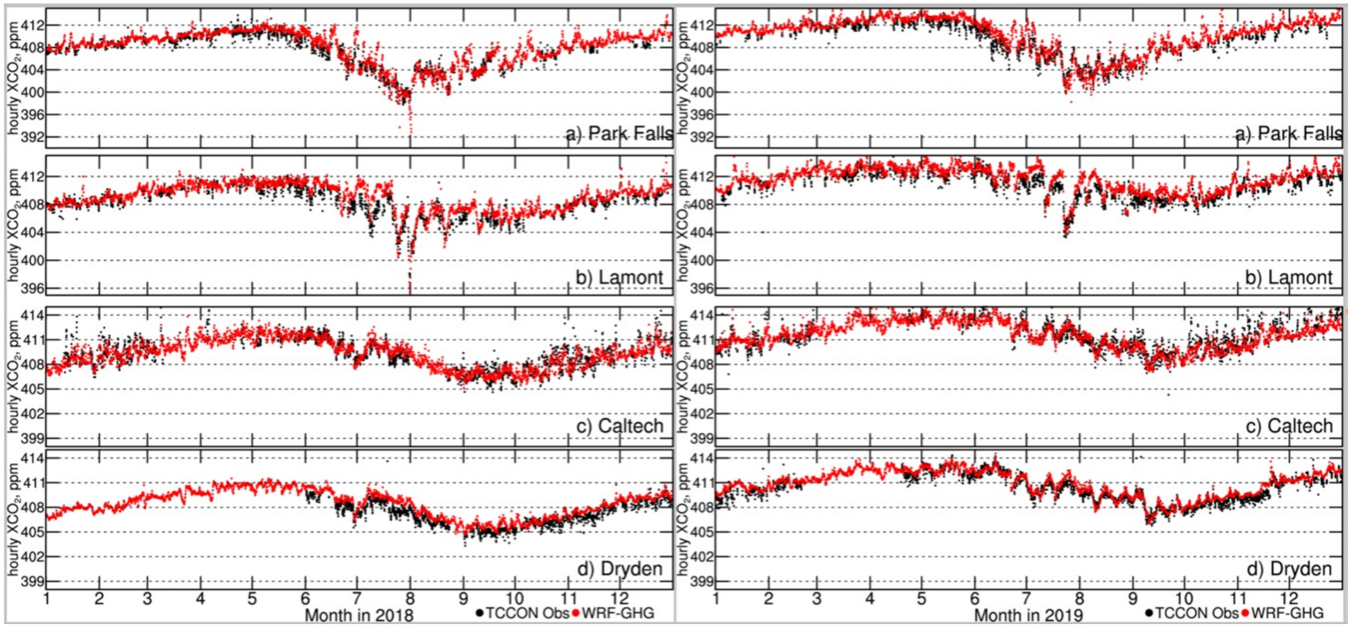

CH_4

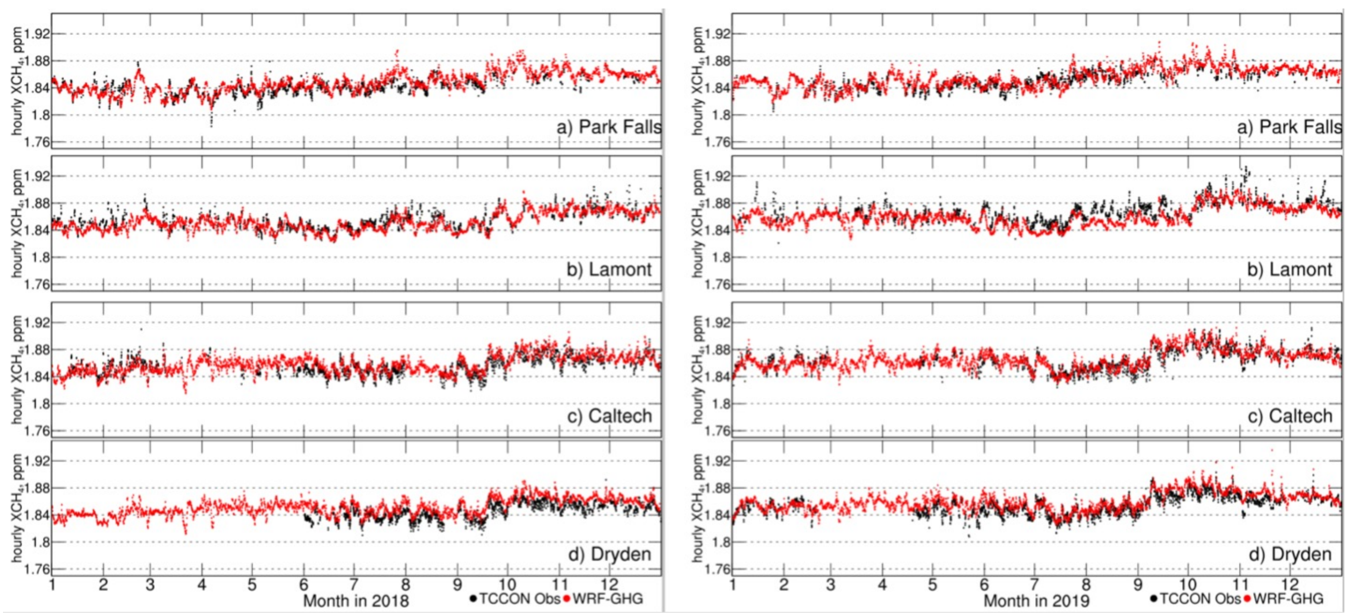

Difference of EVI between 2018 and 2019

June

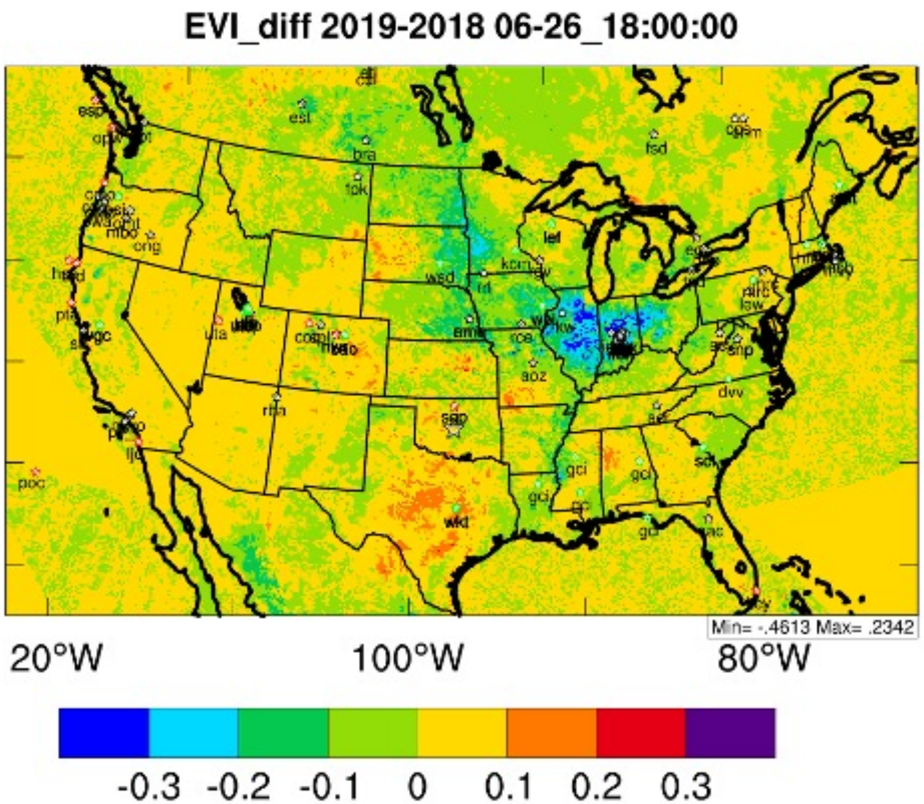

Sept

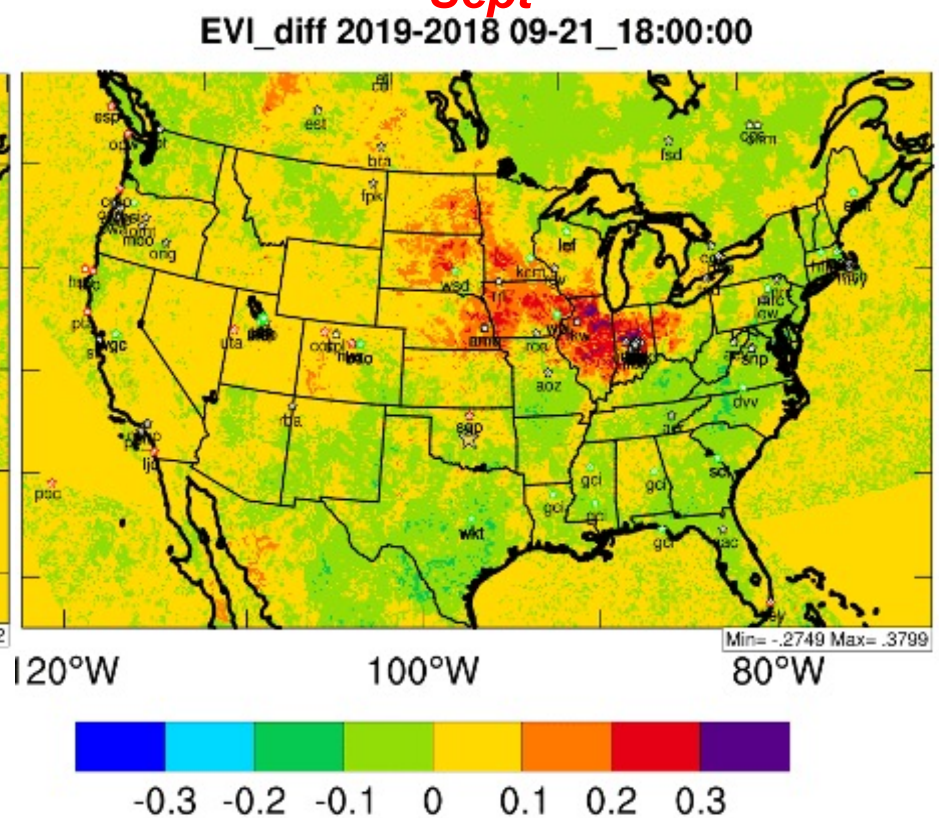

Flood delayed growing season

2019 flood delayed the drawdown of CO_2 in summer

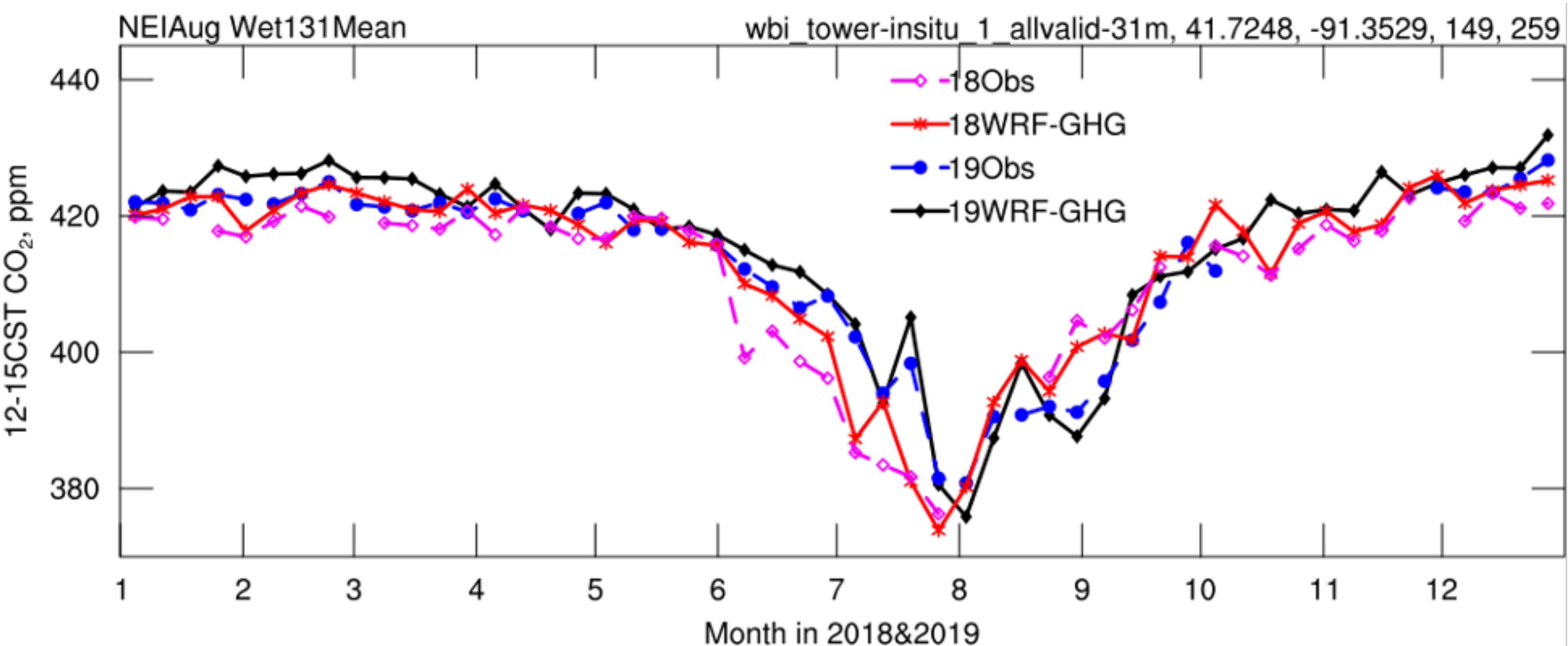

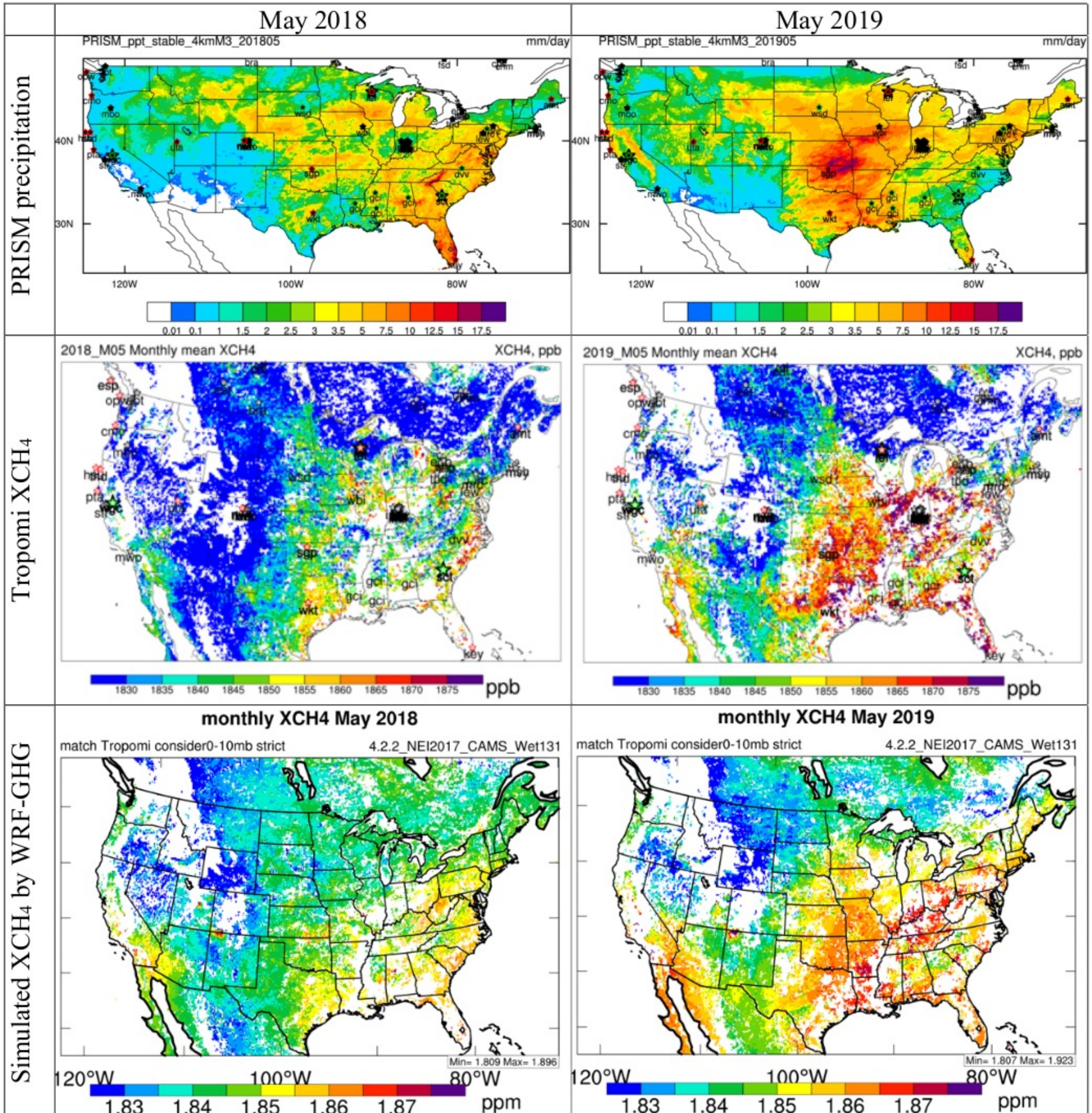
May 2018
May 2019
PRISM precipitation
PRISM_ppt_stable_4kmM3_201805
PRISM_ppt_stable_4kmM3_201905
mm/day
40N
30N
120W
100W
80W
0.01 0.1 1 1.5 2 2.5 3 3.5 5 7.5 10 12.5 15 17.5
Tropomi XCH4
2018_M05 Monthly mean XCH4
2019_M05 Monthly mean XCH4
XCH4, ppb
1830 1835 1840 1845 1850 1855 1860 1865 1870 1875
ppb
Simulated XCH4 by WRF-GHG
monthly XCH4 May 2018
monthly XCH4 May 2019
match Tropomi consider0-10mb strict
4.2.2_NEI2017_CAMS_Wet131
Min= 1.809 Max= 1.896
Min= 1.807 Max= 1.923
120°W
100°W
80°W
1.83 1.84 1.85 1.86 1.87
ppm

CH_4 bias against Obspack due to precipitation bias?

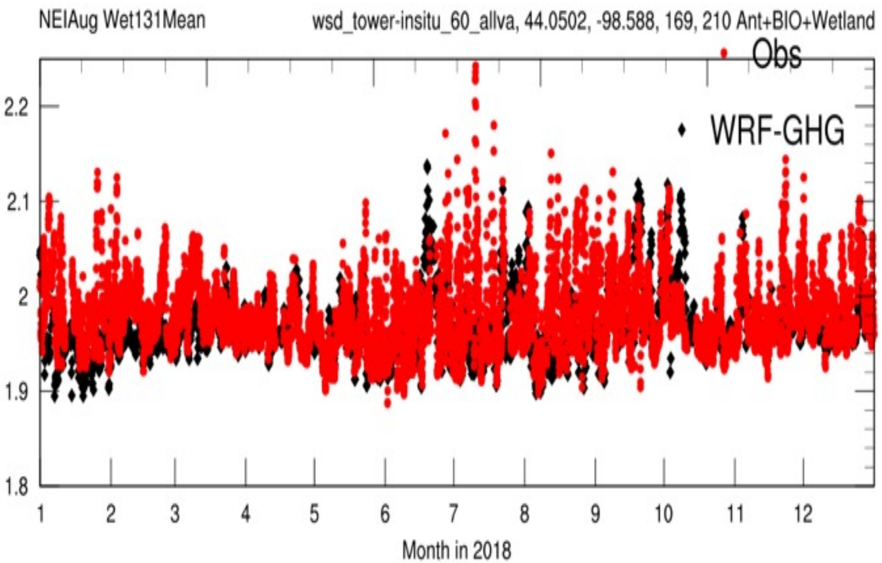

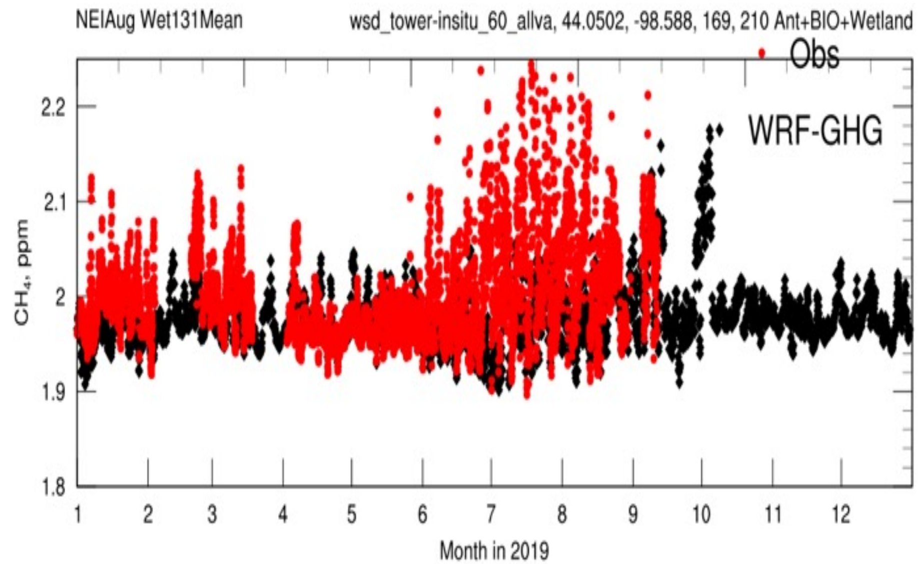

Waiting for PRISM-driven WetCharts CH_4 emission

Summary

1. WRF-GHG is further developed to simulate CO_2 and CH_4.
2. The 2019 May flood delayed growing season in mid-west and the typical spring and summer drawdown of atmospheric CO_2 by 1-3 weeks
3. Obspack and TROPOMI data indicate higher CH_4 in the mid-west in July and August, in 2019 relative to 2018, due to the abnormal precipitation in 2019 in the region that induces more wetland CH_4 emissions.

1. 3D WRF-CO2 simulation

Over US and China

2. Multi-Model investigation of Haze Pollution

3. WRF-GHG for both CO2 and CH4 simulation

4. CH4 inversion

Table 1, Summary of advantages and disadvantages of different top-down flux quantification techniques

flux quantification techniques		Advantages	disadvantages
Conventional simple methods	Mass balance box methods	Simply quantify the emissions using the total flux out of the box covering the emission sources	Require dense spatial sampling or interpolation/extrapolation
	Gaussian plume inversion	Simply quantify the emissions using the Gaussian plume equation	Assume Gaussian distributed plume, which is often not valid in conditions with variable winds and large-scale turbulence
More advanced methods using three-dimensional simulations	Particle dispersion model inversion (also referred to as scaling factor method)	Calculate the emission using the emission-concentration relationship calculated by the dispersion model, good for a single point source	Only scale the pre-assumed emissions without changing the spatial distribution, cannot attribute to different emission locations
More advanced methods through data assimilation	4D-Variational (4D-Var) approach	4D-Var is computationally efficient due to no requirement of ensemble forecast 4D-Var performs well over data sparse regions	Require abjoint model development
	Ensemble Kalman Filter (EnKF)	Quantify emission using flow-dependent error covariance between emissions and concentrations derived from short-term ensemble forecasts Meteorological fields can be simultaneously optimized, which leads to better emission estimation	Need re-cycle ensemble forecasts for time-varying emission sources

Mass balance methods

$$F = \int_{z_1}^{z_2} \int_{x_1}^{x_2} ([CH_4] - [CH_4]_b) U_{\perp} \mathrm{d}x\mathrm{d}z,$$

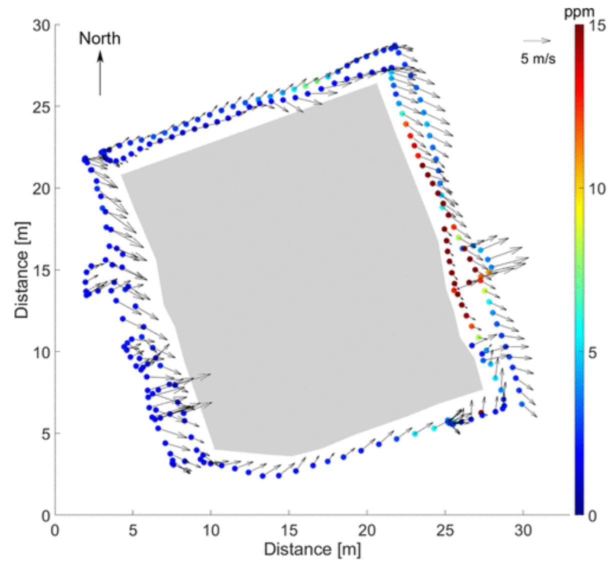

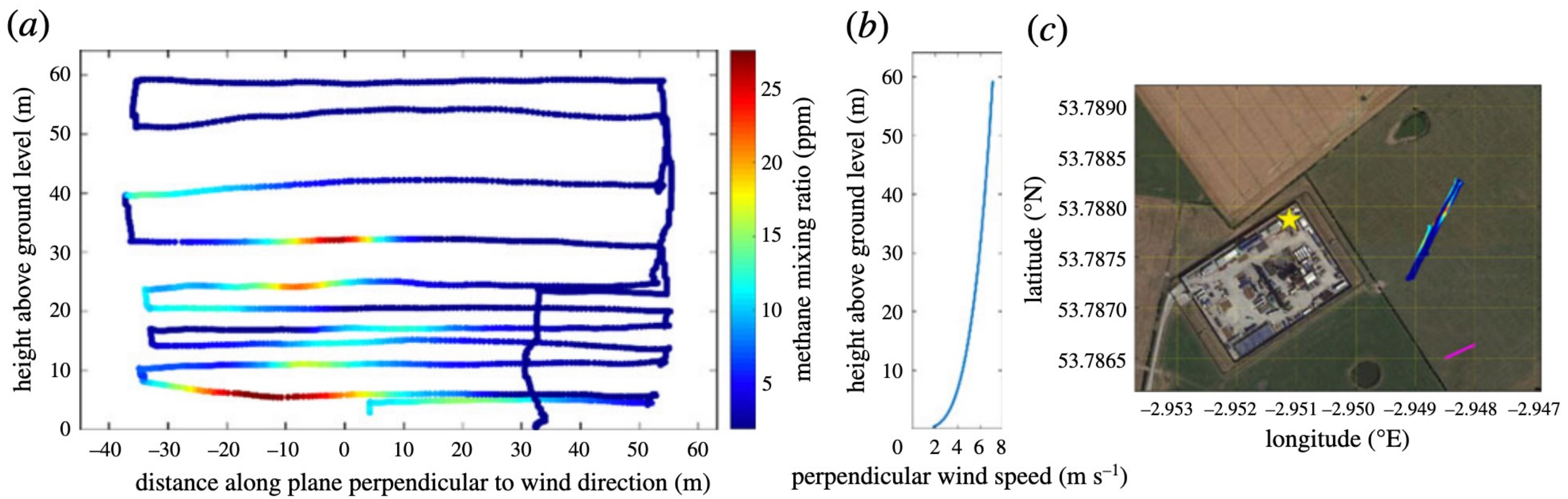

Gaussian plume inversion

$$[CH_4](y,z) = \left(\frac{F}{2\pi U_{\perp} \sigma_y \sigma_z} \times \exp\left(\frac{-y^2}{2{\sigma_y}^2}\right) \times \left(\exp\left(\frac{-(z-H)^2}{2{\sigma_z}^2}\right) + \exp\left(\frac{-(z+H)^2}{2{\sigma_z}^2}\right) \right) \right) + [CH_4]_b,$$

More advance methods using 3D dispersion models and data assimilation

flux quantification techniques		Advantages	disadvantages
Conventional simple methods	Mass balance box methods	Simply quantify the emissions using the total flux out of the box covering the emission sources	Require dense spatial sampling or interpolation/extrapolation
	Gaussian plume inversion	Simply quantify the emissions using the Gaussian plume equation	Assume Gaussian distributed plume, which is often not valid in conditions with variable winds and large-scale turbulence
More advanced methods using three-dimensional simulations	Particle dispersion model inversion (also referred to as scaling factor method)	Calculate the emission using the emission-concentration relationship calculated by the dispersion model, good for a single point source	Only scale the pre-assumed emissions without changing the spatial distribution, cannot attribute to different emission locations
More advanced methods through data assimilation	4D-Variational (4D-Var) approach	4D-Var is computationally efficient due to no requirement of ensemble forecast 4D-Var performs well over data sparse regions	Require abjoint model development
	Ensemble Kalman Filter (EnKF)	Quantify emission using flow-dependent error covariance between emissions and concentrations derived from short-term ensemble forecasts Meteorological fields can be simultaneously optimized, which leads to better emission estimation	Need re-cycle ensemble forecasts for time-varying emission sources

Particle dispersion model inversion (also referred to as scaling factor method)

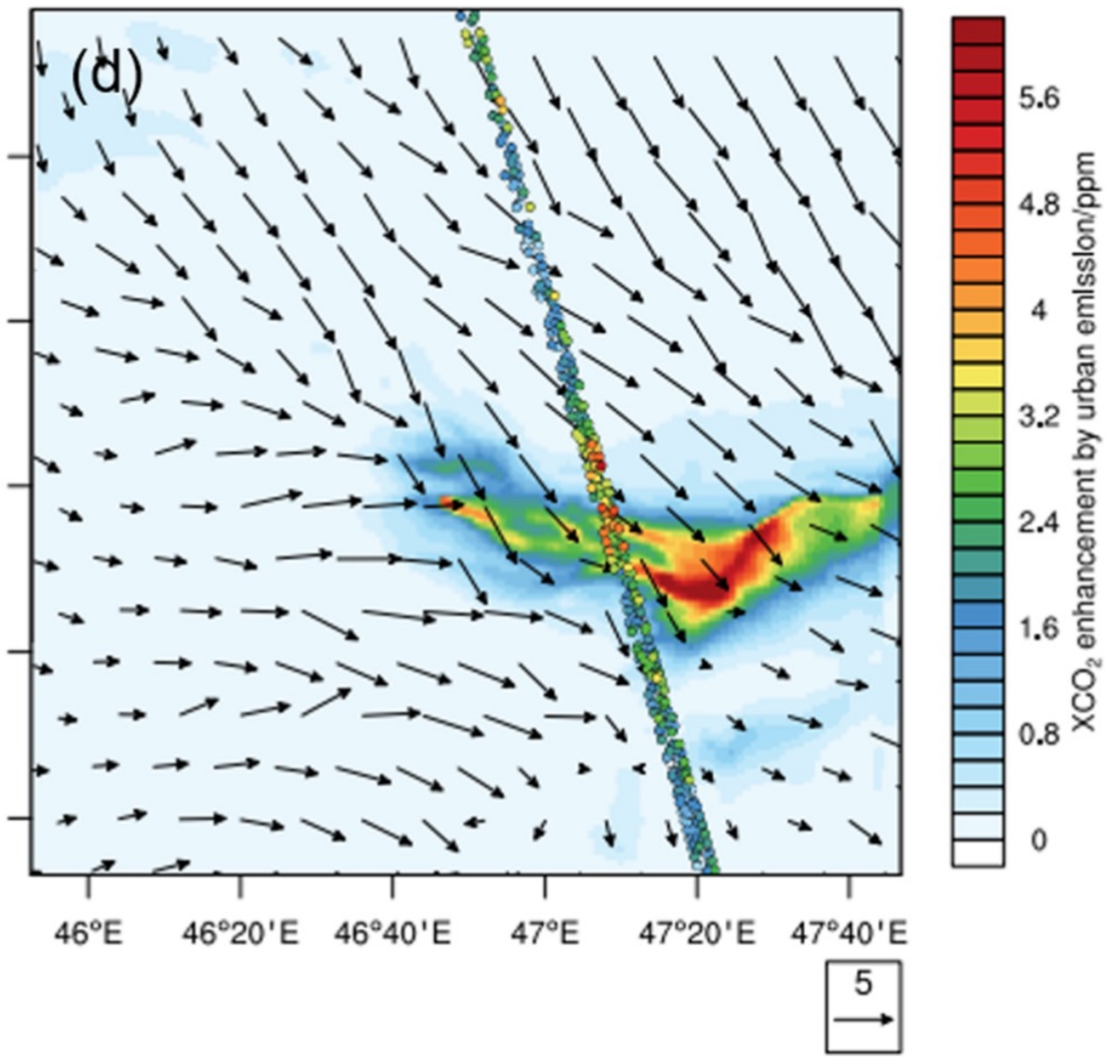

Data assimilation, 4Dvar vs. EnKF

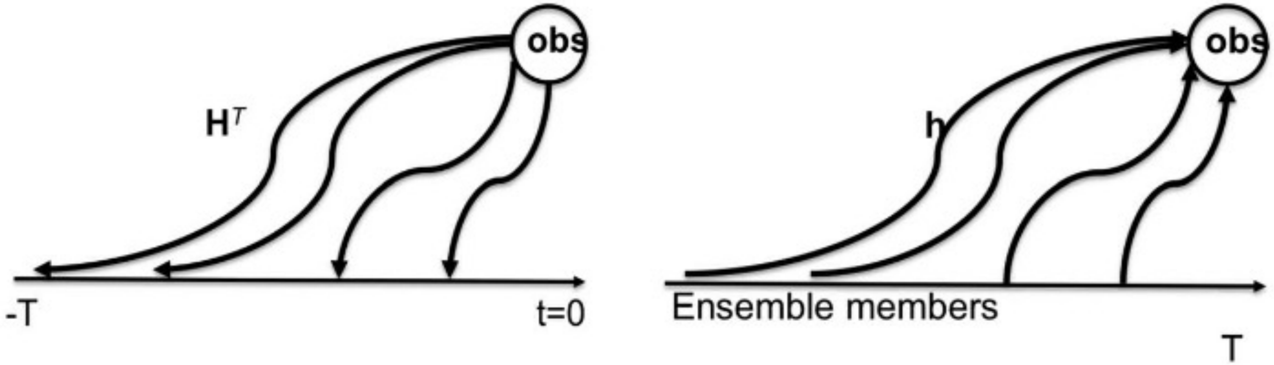

Figure 1. Schematic plot showing the differences between (left) 4D-Var and (right) ensemble Kalman filter in calculating the relationship between CO_2 concentrations and surface fluxes. H^T is the adjoint of the observation operator including the adjoint of transport model, while $h(\cdot)$ represent the forward observation operator including forward transport model.

Hu et al. 2011, GRL

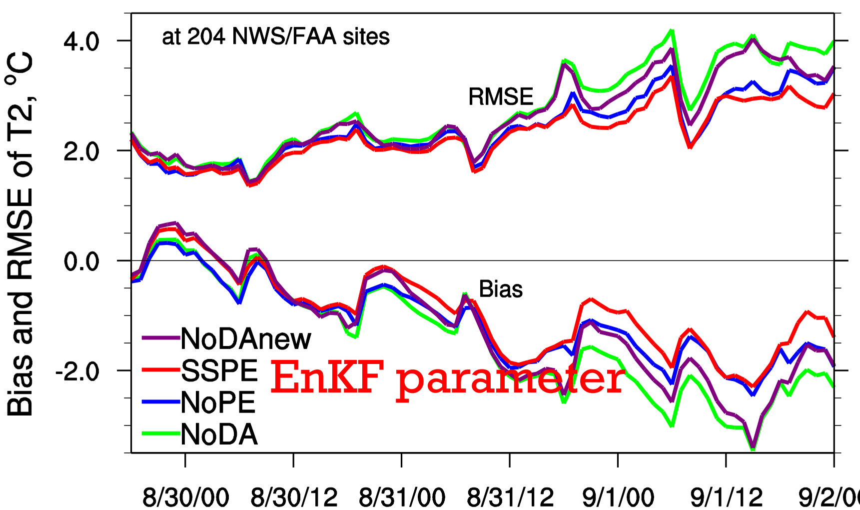

CH4 flux inversion using EnKF-WRF/GHG

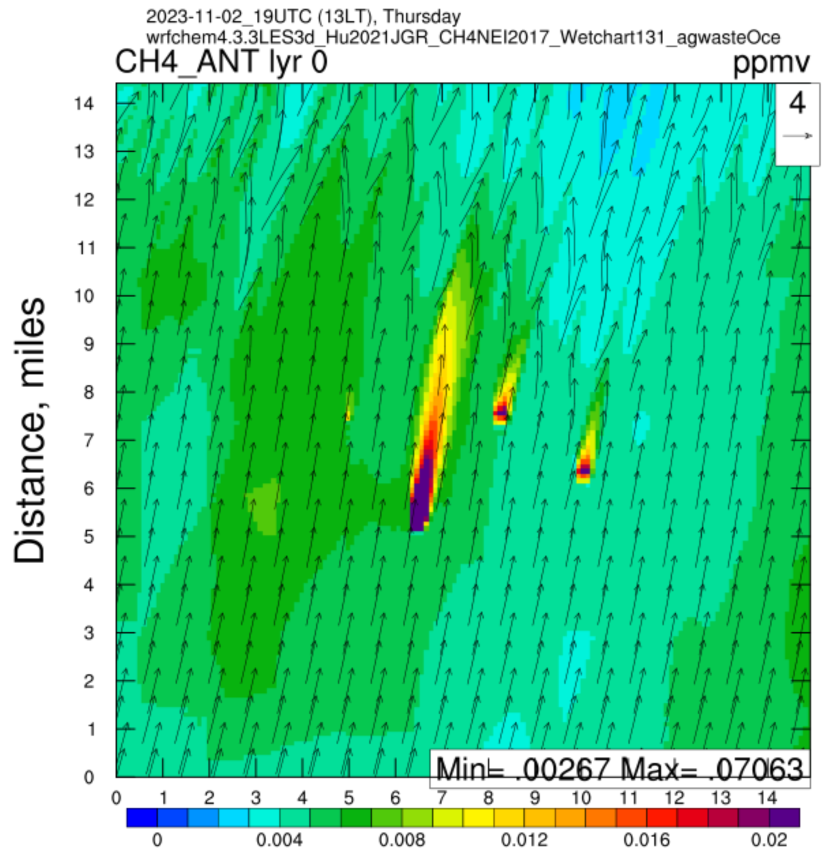

49,248*9 g/day at enlink site and 12,096*9 g/day at devon and El reno site

References

1. **Hu, X.-M.**,Gourdji, S. M., Davis, K. J., Wang, Q., Zhang, Y., Xue, M., . . . Crowell, S. M. R. (2021). Implementation of improved parameterization of terrestrial flux in WRF-VPRM improves the simulation of nighttime CO2 peaks and a daytime CO2 band ahead of a cold front. *JGR: Atmospheres*, e2020JD034362. 10.1029/2020JD034362.
2. **Hu, X.-M.**, S. Crowell, et al. (2020), Dynamical Downscaling of CO_2 in 2016 over the contiguous United States using WRF-VPRM, a weather-biosphere-online-coupled model, *J. Adv. Modeling Earth Systems*, 10.1029/2019MS001875.
3. Li, X., **Hu, X.-M.**, Cai, C. et al. (2020), Terrestrial CO_2 Fluxes, Concentrations, Sources and Budget in Northeast China: Observational and Modeling Studies, *J. Geophys. Res.-Atmospheres*, 10.1029/2019JD031686.
4. **Hu, X.-M.**, J. Hu, L. Gao, C. Cai, Y. Jiang, M. Xue, T. Zhao, and S. M. R. Crowell, 2020: Multi-sensor and multi-model monitoring and investigation of a wintertime air pollution event ahead of a cold front over eastern China. J. Geophy. Res., Conditionally accepted.
5. **Hu, X.-M.**, and M. Xue (2016b), Influence of synoptic sea breeze fronts on the urban heat island intensity in Dallas-Fort Worth, Texas, *Mon. Wea. Rev.*, doi:10.1175/MWR-D-15-0201.1.
6. **Hu, X.-M.**, et al. (2014), Impact of the Loess Plateau on the Atmospheric Boundary Layer Structure and Air Quality in the North China Plain: A Case Study, Science of the Total Environment, 10.1016/j.scitotenv.2014.08.053
7. **Hu, X.-M.**, et al. (2013), Impact of the Vertical Mixing Induced by Low-level Jets on Boundary Layer Ozone Concentration, *Atmos. Environ.*, 70, 123-130
8. **Hu, X.-M.**, J. M. Sigler, and J. D. Fuentes (2010), Variability of ozone in the marine boundary layer of the equatorial Pacific Ocean , *J. of Atmos. Chem.*, 66, 117–136.